Mon. Not. R. Astron. Soc. **392,** 553–569 (2009) doi:10.1111/j.1365-2966.2008.14126.x

Evaluating and improving semi-analytic modelling of dust in galaxies based on radiative transfer calculations

Fabio Fontanot,[1⋆] Rachel S. Somerville,[1] Laura Silva,[2] Pierluigi Monaco[2,3] and Ramin Skibba[1]

[1]*MPIA Max-Planck-Institute für Astronomie, Königstuhl 17, 69117 Heidelberg, Germany*
[2]*INAF-Osservatorio Astronomico, Via Tiepolo 11, I-34131 Trieste, Italy*
[3]*Dipartimento di Astronomia, Università di Trieste, via Tiepolo 11, 34131 Trieste, Italy*

Accepted 2008 October 21. Received 2008 September 19; in original form 2008 May 16

ABSTRACT

The treatment of dust attenuation is crucial in order to compare the predictions of galaxy formation models with multiwavelength observations. Most past studies have used either simple analytic prescriptions or full radiative transfer (RT) calculations. Here, we couple star formation histories and morphologies predicted by the semi-analytic galaxy formation model MORGANA with RT calculations from the spectrophotometric and dust code GRASIL to create a library of galaxy spectral energy distributions from the UV/optical through the far-infrared, and compare the predictions of the RT calculations with analytic prescriptions. We consider a low- and high-redshift sample, as well as an additional library constructed with empirical, non-cosmological star formation histories and simple (pure bulge or disc) morphologies. Based on these libraries, we derive fitting formulae for the effective dust optical depth as a function of galaxy physical properties such as metallicity, gas mass and radius. We show that such fitting formulae can predict the *V*-band optical depth with a scatter smaller than 0.4 dex for both the low- and high-redshift samples, but there is a large galaxy-to-galaxy scatter in the shapes of attenuation curves, probably due to geometrical variations, which our simple recipe does not capture well. However, our new recipe provides a better approximation to the GRASIL results at optical wavelength than standard analytic prescriptions from the literature, particularly at high redshift.

Key words: radiative transfer – dust, extinction – galaxies: evolution.

1 INTRODUCTION

Infrared (IR) observations of galaxies have demonstrated conclusively that dust is a fundamental and ubiquitous component of the interstellar medium (ISM). Dust grains modify the chemical and physical conditions of the ISM by locking up a large fraction of heavy elements ejected by stars, by shielding molecular clouds (MCs) from dissociating radiation, thereby allowing them to cool and condense to the densities necessary to form stars, and by favouring the formation of H_2 molecules themselves on their surfaces (see e.g. the reviews by Dorschner & Henning 1995; Draine 2003). Therefore, dust grains are a fundamental ingredient in the very process of star formation. Also, dust plays a major role in shaping the spectral energy distribution (SED) of galaxies: dust grains absorb and efficiently scatter short wavelength ($\lambda \lesssim 1\,\mu$m) radiation. The extinction efficiency drops steeply for longer wavelength and dust cannot survive at temperatures $\gtrsim$1000 K: the absorbed energy is thermally emitted in the IR. Therefore, dust modifies the intrinsic (pure stellar and/or non-thermal) SED of galaxies. This effect is particularly strong in star-forming regions and starburst galaxies, where the youngest stars are deeply embedded within dense and optically thick dusty cocoons.

The expected link between the intensity of the star formation activity and the amount of dust reprocessing in galaxies has been clearly observed both in the local and in the high-redshift Universe, revealing that much, and in many cases most, of the star formation activity is obscured in the ultraviolet (UV) and optical, and can only be detected in the IR. For example, estimates based on observations with the *IRAS* satellite suggested that globally ∼30 per cent of the bolometric luminosity of nearby galaxies, mostly normal spirals, is reprocessed by dust in the IR (Soifer & Neugebauer 1991; Popescu & Tuffs 2002). But *IRAS* also revealed the existence of a population of heavily obscured luminous and ultraluminous IR galaxies (with $L_{\rm IR} \sim 10^{11}$–$10^{12}\,{\rm L}_{\odot}$, and with $L_{\rm IR} \gtrsim 10^{12}\,{\rm L}_{\odot}$, respectively; e.g. Sanders & Mirabel 1996), and provided a first hint of the strong evolution of these IR bright galaxies. This has been confirmed and quantified to high redshifts with surveys with *ISO* ($z \sim 0.5$–1; Elbaz

⋆E-mail: fontanot@mpia.de

et al. 1999, 2002; Dole et al. 2001; Gruppioni et al. 2002), SCUBA ($z \sim 2$; Smail, Ivison & Blain 1997; Smail et al. 2002; Hughes et al. 1998; Chapman et al. 2005) and *Spitzer* ($z \gtrsim 2$; Le Floc'h et al. 2005; Babbedge et al. 2006). The optical to sub-mm cosmic background radiation provides a measure of the integrated star formation activity taking place at high z. The energy density of the far-infrared (FIR) background measured by *COBE* (Puget et al. 1996; Hauser et al. 1998; Hauser & Dwek 2001) is comparable to that measured in the optical and near-IR (NIR). All these observations indicate that the amount of energy emitted by dust over the history of the Universe is at least comparable to the energy emitted by stars that is able to escape galaxies and reach us, and that star formation activity and the consequent dust reprocessing are much more important at high redshift than locally.

Therefore, the presence and properties of dust in the ISM of galaxies, and its effect on the SEDs, must be considered with care in order to interpret observations to infer basic quantities such as star formation rates (SFR) and masses, as well as to compute reliable predictions (SEDs, luminosity functions, galaxy counts, etc.) from galaxy formation models. The various spectrophotometric codes (PEGASE, Fioc & Rocca-Volmerange 1997; GRASIL, Silva et al. 1998; STARBURST99, Leitherer et al. 1999; Bruzual & Charlot 2003) show reasonable agreement in predictions of the intrinsic, pure stellar SED of a galaxy, given its SFR and metal enrichment history. However, the SED emerging from galaxies is the result of a complex interaction between the intrinsic properties of dust and the relative geometry of the heating sources and the dust. The chemical composition, size distribution and shape of the dust grains determine the absorption and scattering efficiencies of the dust mixture as a function of wavelength. These properties are somewhat constrained only for our galaxy and the Magellanic Clouds through the measurements of the extinction curve and the local diffuse dust emission. But, it is also well known that these extinction curves have different shapes, a fact generally ascribed to different dust properties, and also within each galaxy the curves are spatially variable and dependent on the particular dusty environments sampled by the line of sight (e.g. Mathis, Mezger & Panagia 1983; Rowan-Robinson 1986; Cardelli, Clayton & Mathis 1989; Mathis 1990; Fitzpatrick 1999; Fitzpatrick & Massa 2007). A further issue is the degeneracy among different dust models that reproduce the average extinction curve and cirrus emission in the Milky Way (hereafter MW, see e.g. Draine & Anderson 1985; Desert, Boulanger & Puget 1990; Dwek et al. 1997; Li & Draine 2001; Zubko, Dwek & Arendt 2004).

The relative geometry of stars and dust plays a major role in shaping the SED. This holds both for the attenuated starlight (e.g. Bruzual, Magris & Calvet 1988; Witt, Thronson & Capuano 1992; Efstathiou & Rowan-Robinson 1995; Gordon, Calzetti & Witt 1997; Ferrara et al. 1999; Calzetti 2001) and for the dust emission spectrum. In fact, a fundamental property to be taken into account is that the relative geometry of stars and dust is age-dependent and, therefore, wavelength-dependent, because the youngest stars, which dominate the UV luminosity, are also the most extinguished by the optically thick parent MCs (Silva et al. 1998; Granato et al. 2000; Tuffs et al. 2004). In addition, detailed reproductions of the attenuation properties of disc galaxies seem to require an age-dependent extinction also in the diffuse medium for intermediate age with respect to older stars (Popescu et al. 2000; Panuzzo et al. 2007). All these factors then determine the temperature distribution of the dust grains, with each dusty environment and each dust grain having their own particular response to the radiation field, and therefore yielding the consequent shape of the emerging IR SED.

In order to take full advantage of the wealth of multi-wavelength observations now available to us (UV/optical and IR), galaxy formation models must grapple not only with the modelling of stellar populations, but also with absorption and re-emission by dust. This is equally true for both semi-analytic and numerical hydrodynamic simulations. In semi-analytic models (SAMs; e.g. White & Frenk 1991), the evolution of the dark matter (DM) component is calculated directly using N-body methods or Monte Carlo techniques, while the evolution of the baryonic component is treated by simple recipes for the radiative cooling of gas, star formation, chemical evolution, feedback by supernovae and active galactic nuclei (AGN), etc. (see Baugh 2006 for a review). The SAM provides detailed information about the star formation and enrichment history of each galaxy, but typically only very limited information about the structural properties of the stars, gas and dust (e.g. in general an effective radius can be computed for the disc and spheroid components).

Due to the complexities inherent in the treatment of the radiative effects of dust and the many unknowns connected to the dust properties, most SAMs have made use of simple empirical or phenomenological treatments. A widely adopted approach consists in computing the face-on dust optical depth at a reference wavelength (typically the V band, τ_V), and then computing the inclination dependence assuming that the stars and dust are uniformly mixed in a 'slab' model, and that the wavelength dependence is given by a fixed 'template' attenuation curve. Some modelers (e.g. Kauffmann et al. 1999; Somerville & Primack 1999; Nagashima et al. 2001; Mathis et al. 2002; De Lucia, Kauffmann & White 2004; Kang et al. 2005) compute $\tau_{0,V}$ using empirical relations between galaxy luminosity and dust optical depth (Wang & Heckman 1996). Others assume that $\tau_{0,V}$ is proportional to the column density of dust in the disc, assuming that the dust mass is proportional to the metallicity (Guiderdoni & Rocca-Volmerange 1987, hereafter GRV87; Lacey et al. 1993; Guiderdoni et al. 1998; Devriendt & Guiderdoni 2000; Hatton et al. 2003; Blaizot et al. 2004; Kitzbichler & White 2007). De Lucia & Blaizot (2007) (hereafter DLB07) adopt the latter prescription for obscuration due to the diffuse 'cirrus' component, coupled with the approach suggested by Charlot & Fall (2000) (hereafter CF00) to account for the larger obscuration of the youngest stars by the molecular birth clouds. Cole et al. (2000) and Bell et al. (2003) instead couple their SAM with the Ferrara et al. (1999) library, which provides the net attenuation for smooth distributions of stars and dust as a function of wavelength and inclination angle based on radiative transfer (RT) calculations.

In some papers, the IR properties of galaxies in SAMs are also computed. Using one of the above methods for computing the optical depth and attenuation curve, and hence the total amount of energy absorbed by the dust, and assuming that all of this light is re-radiated in the IR, one can use observationally calibrated templates describing the wavelength dependence of the dust emission (Guiderdoni et al. 1998; Devriendt, Guiderdoni & Sadat 1999; Devriendt & Guiderdoni 2000; Hatton et al. 2003; Blaizot et al. 2004), or modified Planck functions (e.g. Kaviani, Haehnelt & Kauffmann 2003) to compute IR luminosities. In a few cases, SAMs have instead been coupled with a self-consistent RT calculation for the full (UV to sub-mm) SED [see e.g. Granato et al. (2000); Baugh et al. (2005); Lacey et al. (2008, GALFORM); Fontanot et al. (2007, MORGANA); Granato et al. (2004); Silva et al. (2005)].

Clearly, there is a large range in both complexity and computation time represented in the treatments of dust in galaxy formation models in the literature. On the one hand, it is natural to be dubious that a simple empirical approach can adequately represent the intricacies of this very messy process. On the other hand, one of the advantages

of SAMs is their flexibility and computational efficiency, and this advantage is substantially undermined if one chooses to do full RT calculations for each galaxy. Moreover, given that SAMs are anyway based on a series of approximations, and that so many details of the relevant physics of galaxy formation (structural properties, star formation, chemical evolution, supernova and AGN feedback) are poorly understood and crudely modelled, feeding the results of SAMs into full RT may not be well motivated.

In this paper, we make use of libraries of RT calculations based on SAM outputs as well as sets of non-cosmological, empirical star formation/enrichment histories to address the following questions. (1) How different are the results from the simple analytic dust models and the full RT calculations? (2) How do the predictions from the RT calculations depend on the physical properties of the model galaxies? (3) Can we derive an improved analytic recipe, based on the RT calculations, that can be efficiently implemented in SAMs? The SAM that we use for this study is the MORGANA model (Fontanot et al. 2006, 2007; Monaco, Fontanot & Taffoni 2007), and the RT libraries are constructed using the GRASIL code (Silva et al. 1998; Silva 1999).

MORGANA produces good overall agreement with observations of galaxy properties; any discrepancy is of little concern in this context, since in principle we could proceed by simply comparing SEDs resulting from different dust prescriptions applied to any possible realizations of the SAM. However, we wish to disentangle the dependence of the dust extinction predictions on galaxy physical properties from the correlations between these properties, and from distributions of these properties characteristic of a given cosmic epoch, as predicted by MORGANA or present in the real Universe. Therefore, we construct an 'empirical' library, based on a classical 'open box' chemical evolution code with simple parametrized star formation histories, chosen to span the broadest range of possibilities. In addition, we consider both high- and low-redshift catalogues extracted from the MORGANA outputs. In fact, we may expect that locally calibrated simple dust prescriptions will give acceptable results when coupled to a model characterized by a globally good agreement with local galaxy populations. Instead, this may not be the case at high z, where galaxies will typically have properties different from local ones. We focus on predictions of commonly used quantities in galaxy formation studies, namely rest-frame magnitudes in the near-UV through NIR [Sloan Digital Sky Survey (SDSS) *ugri* and 2MASS *K* band]. IR luminosities from the mid-IR (3.5 μm) to the sub-mm will be the focus of a companion paper (Fontanot et al., in preparation).

This paper is organized as follows. In Section 2, we describe the main features of the MORGANA and GRASIL models and the construction of the RT-based libraries that we will use for our comparison. In Section 3, we define some useful notation and summarize the analytic prescriptions for dust attenuation that we will evaluate. In Section 4, we derive fitting formulae between physical galaxy properties and the dust effective optical depth. In Section 5, we present our analysis of the results of the RT calculations in terms of physical properties, and a comparison of the RT predictions at UV/optical/NIR wavelengths with several analytic prescriptions. We give our conclusions in Section 6. Throughout this paper, we use magnitudes in the AB system (unless otherwise stated).

2 GALAXY MODELS AND RT LIBRARIES

The required inputs to the RT-based GRASIL model are the unextinguished stellar SED and the geometry and relative distribution of stars and dust. We assume that galaxies can be represented by a simple composite geometry of spheroid plus disc, and that both components are axisymmetric. The spheroid is represented by a King profile, and the disc by a radial and vertical exponential profile. The stellar SED is computed by convolving the distribution of stellar ages and metallicities arising from a given star formation and enrichment history with simple stellar population (SSP) models (Bressan, Granato & Silva 1998; Bressan, Silva & Granato 2002). The star formation histories, and hence stellar SEDs, are tracked separately for the bulge and disc components. We describe the details of how these quantities are obtained for each of our libraries in the following sections.

We make use of two different approaches to obtain ensembles of these input parameters. The first approach is based on semi-analytic simulations with the MORGANA code (details given in Section 2.1) within the Λcold dark matter cosmological context. We extract catalogues at both low and high redshift from MORGANA. We refer to the libraries that are obtained from the MORGANA outputs as the *Morgana Library* (ML). In addition, we create a library in which the star formation/enrichment histories are predicted by MORGANA as before, but instead of having a composite disc+spheroid morphology, disc-dominated galaxies are represented as a pure disc and bulge-dominated galaxies as a pure bulge. In this way, we can attempt to disentangle the effects of geometry and star formation history. We refer to this as the *Control Library* (CL).

For the second approach, we use a classical chemical evolution code (CHE_EVO), which is not embedded in a cosmological context (details are given in Section 2.2). The goal is to remove the 'prior' that is contained in the cosmological models, in the form of the predicted correlations between and distributions of physical parameters. We refer to this as *Empirical Library* (EL).

All libraries assume a Salpeter (1955) IMF with mass range from 0.1 to 100 $M_{\odot}$. Table 1 summarizes the different libraries considered in this paper and described in this section.

2.1 Semi-analytic galaxy formation model: MORGANA

MORGANA (MOdel for the Rise of GAlaxies aNd Active nuclei) is a SAM for the formation and evolution of galaxies and AGN (Fontanot et al. 2006, 2007; Monaco et al. 2007). The main characteristics and ingredients it implements are as follows: (i) a sophisticated treatment of the mass and energy flows between galactic phases (cold and hot gas, stars) and components (bulge, disc and halo) coupled with the multi-phase treatment of the interstellar and intra-cluster media; (ii) an improved modelling of cooling and infall (Viola et al. 2008); (iii) a multi-phase description of star formation and feedback processes (Monaco 2004); (iv) a self-consistent description of AGN activity and feedback (Fontanot et al. 2006) and (v) the building of the diffuse stellar component in galaxy cluster from the stars scattered in galaxy mergers (Monaco et al. 2006).

The MORGANA realization from which we extract the library of star formation histories considered here, the ML, is the same presented in Fontanot et al. (2007), and we refer to that paper for more details. It shows good agreement with the local stellar mass function, cosmic star formation history, the evolution of the stellar mass density, the slope and normalization of the Tully–Fisher relation for spiral discs, the redshift distributions and luminosity function evolution of *K*-band-selected samples and the 850 μm number counts. Despite the fact that this model is able to reproduce the overall assembly of massive galaxies, it does not reproduce the 'downsizing' trend of galaxies: in particular, it overpredicts the number of bright galaxies at $z < 1$ (Monaco et al. 2006) and the number of faint galaxies at $z \geq 1$ (Fontana et al. 2006). Moreover, the model still underpredicts

Table 1. Summary of RT libraries used in our comparison.

Sample name	Star formation history	Geometry	Redshift interval
ML – disc-dominated – low z	MORGANA	Disc+bulge	$0.0 < z < 0.2$
ML – bulge-dominated – low z	MORGANA	Disc+bulge	$0.0 < z < 0.2$
ML – disc-dominated – high z	MORGANA	Disc+bulge	$2.0 < z < 3.0$
ML – bulge-dominated – high z	MORGANA	Disc+bulge	$2.0 < z < 3.0$
CL – disc-dominated – low z	MORGANA	Pure disc	$0.0 < z < 0.2$
CL – bulge-dominated – low z	MORGANA	Pure bulge	$0.0 < z < 0.2$
CL – disc-dominated – high z	MORGANA	Pure disc	$2.0 < z < 3.0$
CL – bulge-dominated – high z	MORGANA	Pure bulge	$2.0 < z < 3.0$
EL – disc-dominated	CHE_EVO	Pure disc	–
EL – bulge-dominated	CHE_EVO	Pure bulge	–

the counts of the brightest 850 μm galaxies at high z. In this model, we neglect other ingredients, such as quasar-triggered galactic winds (see Monaco & Fontanot 2005). We checked that including these ingredients does not change the conclusions presented in this paper.

MORGANA gives predictions for the star formation histories of disc and bulge components separately, and for galaxy sizes. Disc sizes are computed using the Mo, Mao & White (1998) approach. The spin parameter of the DM halo is randomly chosen from its known distribution, and it is assumed that the angular momentum is conserved. The presence of a central bulge is taken into account in computing the disc size. Bulge sizes are computed (as e.g. in Cole et al. 2000) by assuming that kinetic energy is conserved when the merger of two collisionless discs takes place. We classify the objects in the ML into two categories according to the stellar *bulge-to-total* mass ratio $\mathrm{B/T} = \frac{M_{\rm bulge}}{M_{\rm bulge}+M_{\rm disc}}$. Following Madgwick et al. (2003), we assume bulge-dominated galaxies to correspond to $\mathrm{B/T} > 0.6$, and disc-dominated to $\mathrm{B/T} \leq 0.6$.

We compare the physical properties of our model galaxies with the SDSS sample, and in particular with the specific star formation $r_{\rm SFR} = \mathrm{SFR}/M_\star$ versus stellar mass $M_\star$ plot presented in Brinchmann et al. (2004). They find that massive galaxies show low $r_{\rm SFR}$ values, whereas less massive galaxies populate a horizontal strip in the diagram, corresponding to higher $r_{\rm SFR}$ values. Moreover, Madgwick et al. (2003) find a relation between the morphological type and $r_{\rm SFR}$: objects with $\log(r_{\rm rsf}) < -11$ [$\log(r_{\rm rsf}) > -11$] tend to be bulge-(disc-) dominated galaxies. We show the corresponding plot for the objects in the ML in Fig. 1; we mark the position of bulge-(disc-) dominated galaxies as red crosses (cyan circles). It is evident from this plot that the massive objects in MORGANA favour a bulge-dominated morphology, whereas the low-mass tail is populated by a large fraction of disc-dominated objects, in qualitative agreement with the SDSS observations. However, many massive galaxies show residual star formation activity, which is not seen in the SDSS data: this is likely due to the incomplete quenching of cooling flows at late times in MORGANA (see Monaco et al. 2007 for a complete discussion of this point). Moreover, the star formation activity of many disc-dominated galaxies is too low with respect to observations, in part likely due to the strangulation processes acting on cluster satellite galaxies. However, these residual discrepancies between observations and model are not a major issue for this paper.

Many relevant properties of galaxies, such as the SFR and sizes, evolve with redshift. We consider two samples drawn from MORGANA, a 'low-z' sample at $z < 0.20$ and a 'high-z' sample at

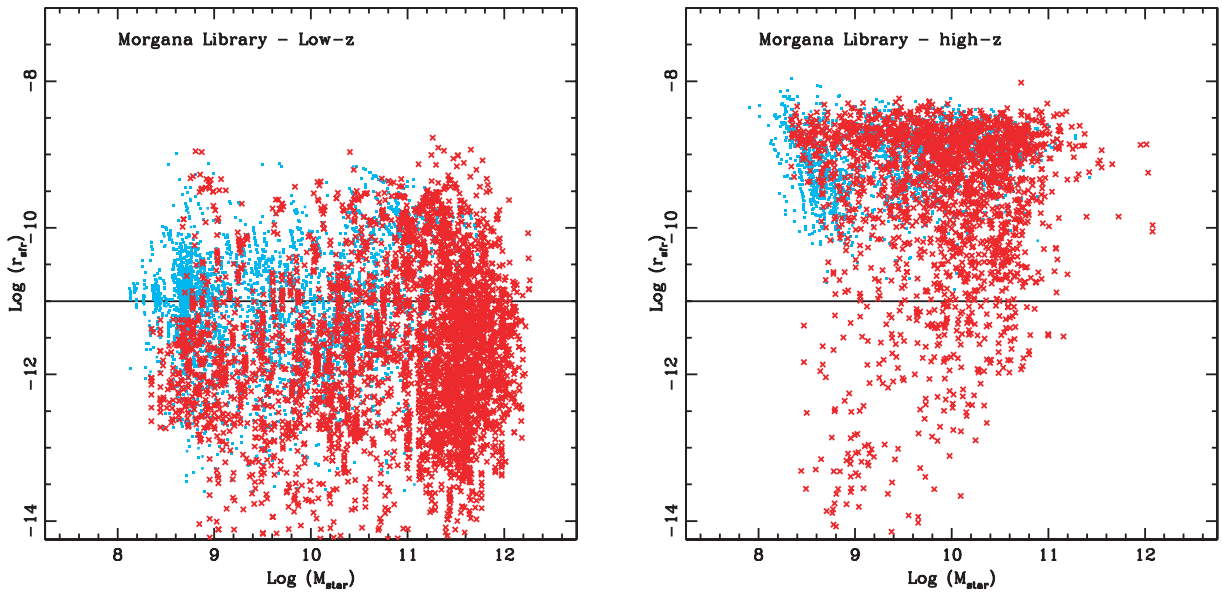

Figure 1. $\log(M_\star/\mathrm{M}_\odot)$ versus $\log(r_{\rm SFR}/\mathrm{yr}^{-1})$ for the MORGANA library (ML). Red crosses and cyan circles refer, respectively, to bulge-dominated and disc-dominated objects. Left- and right-hand panels refer to the low- and high-z sample, respectively.

$2.0 < z < 3.0$. In the following, we will refer to the libraries based on these two samples as the 'low-z' and 'high-z' libraries. For both libraries, we define disc- and bulge-dominated sub-samples. Starting from these samples we also define the CL accordingly.

2.2 Simple star formation history model: CHE_EVO

In order to explore the correlation between dust attenuation and the physical properties of model galaxies, we need to define a different sort of model library. The recipes that determine galaxy evolution in MORGANA (star formation, feedback, etc.) are responsible for built-in correlations among the physical quantities that enter in the determination of dust attenuation (metallicity, mass of gas and/or stars, SFR, radius of the galaxy, bolometric luminosity). These recipes (and their induced correlations) differ from SAM to SAM. In order to make sure our results are independent of the particular SAM we consider, we define another library, EL, using the chemical evolution code CHE_EVO (Silva 1999).

This is a 'classical open box' chemical evolution code to compute the star formation and metallicity evolution of galaxies, with the following characteristics. (i) The gas from which stars form has an infall rate given by an exponential function of time with an e-folding time $\tau_{\rm infall}$. The normalization of the gas infall rate is fixed by setting the total mass $M_{\rm infall}$ at a given time $t_{\rm infall}$. (ii) The SFR can be expressed as a function of the mass of gas, as an arbitrary function of time or as a combination of both $\mathrm{SFR}(t) = \nu_{\rm sch} M_{\rm gas}(t)^{k_{\rm sch}} + f(t; M_{\rm gas})$, where the first term is a Schmidt-type law with efficiency $\nu_{\rm sch}$, and exponent $k_{\rm sch}$. The second term represents a superimposed mode for which we set the initial and final time t_1 and t_2 and the fraction of gas converted into stars $f_\star$. We choose two possibilities for this mode: an exponential form depending only on time with e-folding time $e_\star$ and a 'Schmidt enhanced' mode, with efficiency $\epsilon_{\rm sch-en}$ and exponent $\alpha_{\rm sch-en}$. (iii) It is possible to set a time $t_{\rm wind}$ to represent the development of a galactic wind after which all the gas is removed, and the SFR and infall are stopped. All the gas present after this age comes from stellar evolution. (iv) The metallicity evolution $Z(t)$ is computed by accounting for the lifetimes and yields of stars as a function of their mass and metallicity, including also Type Ia supernovae. The evolution of all the quantities is then computed to a final age $t_{\rm fin}$.

In order to define a library with a uniform coverage of the possible evolutionary histories, we randomly extract the values of most of the CHE_EVO parameters within large intervals, as reported in Table 2. For each combination of those parameters we consider $t_{\rm fin} = 5$, 10, 13.6 Gyr. We fix $t_{\rm infall} = 13$ Gyr (which sets the normalization of the infall rate), $k_{\rm sch} = 1$, $\alpha_{\rm sch-en} = 1$, since their variation does not add further information. In order to break possible remaining correlations, we then renormalize separately the star formation history and the evolution of the cold gas mass to final values extracted randomly from uniform distributions. This choice forces the final metallicity evolution to be independent of the star formation history and the cold gas content. The final result of this procedure is a uniform distribution of the models in the (SFR, $M_{\rm gas}$, Z) space. We then randomly assign simple morphologies (i.e. pure disc or pure bulge) to the objects in the EL. We also recompute the EL using the Madgwick et al. (2003) criterion for assigning morphologies based on their specific SFR: we assume that objects with $\log(r_{\rm SFR}) < -11$ correspond to pure spheroidal galaxies, and objects with $\log(r_{\rm SFR}) \geq -11$ are considered to be pure discs. We have checked that our conclusions do not change between the two libraries, so we will present results only for the first realization.

Table 2. Parameters for the generation of random star formation histories with CHE_EVO.

Parameter	Lower value	Upper value
$t_{\rm wind}$	1 Gyr	15 Gyr
t_1	3 Gyr	10 Gyr
t_2	t_1	$t_1 + 7$ Gyr
$M_{\rm infall}$	$10^7\,\mathrm{M}_\odot$	$10^{14}\,\mathrm{M}_\odot$
$\tau_{\rm infall}$	5 Gyr	10 Gyr
$f_\star$	0	1
$e_\star$	0 Gyr	7 Gyr
$\epsilon_{\rm sch-en}$	0	10

2.3 Dust and radiative transfer model: GRASIL

For each object in the MORGANA and CHE_EVO libraries, we compute the corresponding UV to radio SED using the spectrophotometric code GRASIL (Silva et al. 1998). Subsequent updates and improvements are described in full detail in Silva (1999), Granato et al. (2000), Bressan et al. (2002), Panuzzo et al. (2003) and Vega et al. (2005). We refer to these papers for more details.

GRASIL solves the equation of RT, taking into account a state-of-the-art treatment of dust effects, and includes the following main features: (i) stars and dust are distributed in a bulge (King profile) + disc (radial and vertical exponential profiles) axisymmetric geometry; (ii) the clumping of both (young) stars and dust through a two-phase ISM with dense giant star-forming MCs embedded in a diffuse ('cirrus') phase is considered; (iii) the stars are assumed to be born within the optically thick MCs and to gradually escape from them on a time-scale $t_{\rm esc}$, this gives rise to the age-(wavelength-) dependent extinction with the youngest and most luminous stars suffering larger extinction than older ones; (iv) the dust composition consists of graphite and silicate grains with a distribution of grain sizes, and Polycyclic Aromatic Hydrocarbons (PAH) molecules; (v) at each point within the galaxy and for each grain type the appropriate temperature T is computed (either the equilibrium T for big grains or a probability distribution for small grains and PAHs); (vi) the RT of starlight through dust is computed along the required line of sight yielding the emerging SED and (vii) the SSP library (Bressan et al. 1998, 2002) includes the effect of the dusty envelopes around AGB stars, and the radio emission from synchrotron radiation and from ionized gas in H II regions.

For the MORGANA+GRASIL library (ML or CL), the scale radii for stars and dust in the disc ($r_{\rm d}^\star$, $r_{\rm d}^d$) and in the bulge ($r_{\rm b}^\star$, $r_{\rm b}^d$) are provided by MORGANA. The disc scaleheights for stars and dust ($h_{\rm d}^\star$ and $h_{\rm d}^d$) are set to 0.1 times the corresponding scale radii.

For the CHE_EVO+GRASIL library (EL), we assume that the scale radius depends on stellar mass as

$$r = k_{\rm r}\alpha_{\rm r}\left(\frac{M_\star}{10^{11}\,\mathrm{M}_\odot}\right)^{1/3}\ \mathrm{kpc} \qquad (1)$$

where $\alpha_{\rm r} = 0.2$ kpc for $r_{\rm b}^\star$, $\alpha_{\rm r} = 3.0$ kpc for $r_{\rm d}^\star$ and $k_{\rm r}$ is a random number between 0.5 and 2. We assume the same scale radii for the stellar and dust components and set the disc scaleheights to 0.1 times the corresponding scale radii.

We fixed the other parameters needed by GRASIL and not provided by the star formation models. (i) The escape time-scale of young stars for the parent MCs is set to $t_{\rm esc} = 10^7$ yr, an intermediate value between that found by Silva et al. (1998) to describe well the SED of spirals ($\sim$ a few Myr) and starbursts ($\sim$ a few 10 Myr), and of the order of the estimated destruction time-scale of MCs by massive stars. In Fontanot et al. (2007), this value was found

to produce good agreement with the *K*-band luminosity functions and the 850 μm counts. (ii) The gas mass predicted by MORGANA or CHE_EVO is subdivided between the dense and diffuse phases, assuming the fraction of gas in the star-forming MCs $f_{\rm MC}$ is 0.5. The results are not very sensitive to this choice. (iii) The mass of dust is obtained by the gas mass and the dust-to-gas mass ratio $\delta_{\rm dust}$ which is set to evolve linearly with the metallicity given by the galaxy model, $\delta_{\rm dust} = 0.45\,Z$. (iv) The optical depth of MCs depends on the ratio $\tau_{\rm MC} \propto \delta_{\rm dust} M_{\rm MC}/r_{\rm MC}^2$; we set the mass and radius of MCs to typical values for the MW, $M_{\rm MC} = 10^6\,{\rm M}_\odot$ and $r_{\rm MC} = 16$ pc. (iv) The dust grain size distribution and composition are chosen to match the mean MW extinction curve.

GRASIL computes the resulting SEDs along different lines of sight, but in the following we use only angle-averaged SEDs, unless otherwise stated. We convolve the SEDs with the GALEX FUV, SDSS *u*, *g*, *r*, *i* and 2MASS K_s filters.

3 ANALYTIC AND EMPIRICAL PRESCRIPTIONS FOR ATTENUATION

3.1 Definitions and notation

For clarity, we first define some useful notation and the meaning of several quantities that we will use throughout the remainder of the paper.

The amount and wavelength dependence of the dust attenuation on the intrinsic (pure stellar) SED of a system are commonly defined through the ratio between the emerging (after interaction with dust) and intrinsic luminosity, typically expressed in magnitudes:

$$A_\lambda \equiv m_\lambda - m_\lambda^0 = -2.5\,\log L_\lambda/L_\lambda^0. \quad (2)$$

It is important to clearly define and explicitly distinguish between the *extinction* and the *attenuation* curve (e.g. Granato et al. 2000; Calzetti 2001). The term *extinction* is commonly used to describe the wavelength dependence of the optical properties (absorption plus scattering) of the dust mixture. Indeed, in the simple geometrical configuration of a slab of dust between the observer and a point source, as is the case when directly measuring the extinction from observations of background stars, since the dust emission along the line of sight (both true dust emission and scattering) is negligible within a point source image, the solution of the equation of RT provides a direct link between the ratio of the observed to intrinsic energy, and the dust optical depth: $L_\lambda/L_\lambda^0 = \exp(-\tau_\lambda)$. Therefore, in this case, $A_\lambda = 1.086\,\tau_\lambda$, where $\tau_\lambda = \tau_{\lambda,\rm abs} + \tau_{\lambda,\rm sca}$ contains the information on the dust properties along the line of sight.

This simple situation of course does not apply to studies of external galaxies. In this case, we refer to A_λ as the *attenuation* curve (other commonly used terms with the same meaning are obscuration, effective extinction or absorption), since in this case the solution of the RT equation does not provide either a simple or a priori predictable relation for L_λ/L_λ^0. For convenience, it is a common practice to define an 'effective' optical depth such that $L_\lambda/L_\lambda^0 = \exp(-\tau_\lambda^{\rm eff})$, with $\tau_\lambda^{\rm eff}$ summarizing the complex interaction between stars and dust in galaxies. This is further discussed in Section 5.1.

In the following, we refer to these quantities, the attenuation and the corresponding effective optical depth obtained with GRASIL, as $A_\lambda^{\rm GS}$, $\tau_\lambda^{\rm GS}$, and the colour excess as

$$E^{\rm GS}(\lambda_1 - \lambda_2) = A_{\lambda_1}^{\rm GS} - A_{\lambda_2}^{\rm GS}. \quad (3)$$

We will compare the values of these quantities obtained from GRASIL with those that we obtain when we apply various analytic dust prescriptions to the pure stellar SED.

3.2 Analytic prescriptions for attenuation

Several simple and computationally efficient treatments of dust effects in galactic SEDs have been proposed. They adopt different approaches to the problem, making a direct comparison difficult. However, they also share some basic ingredients: (1) an attenuation law, either empirical (e.g. Calzetti, Kinney & Storchi-Bergmann 1994; Calzetti et al. 2000) or obtained by coupling an extinction law with an idealized geometrical configuration; (2) a face-on effective optical depth at a reference wavelength (usually *V* band) and (3) a geometrical model for the dependence of the attenuation on viewing angle. Below, we describe some of the most commonly adopted prescriptions for these ingredients, focusing on those that we will compare with in the next section.

3.3 Extinction and attenuation laws

For our own and a few nearby galaxies, the extinction law of the dust has been directly measured from observations of background stars. The differences found between the shapes of the (average) extinction curves of the Galaxy, the Large Magellanic Cloud and the Small Magellanic Cloud below ∼2600 Å are often ascribed to the different metallicities in these systems. The Galactic extinction curve for the diffuse medium is commonly adopted (e.g. Mathis et al. 1983; Fitzpatrick 1989).

Calzetti et al. (1994, 2000) have analysed the dust attenuation for a sample of UV-bright starbursts. The derived attenuation curve is characterized by a shallower UV slope than that of the MW extinction, and by the absence of the 2175 Å feature. A complementary method of defining an empirical attenuation law has been presented by CF00. They consider an attenuation curve that is a power-law function of wavelength, with a normalization that depends on the age of the stellar population:

$$\tau_\lambda^{\rm CF} = \begin{cases} \tau_V(\lambda/5500\,{\rm Å})^{-0.7} & \text{if } t \le t_{\rm MC} \\ \mu\,\tau_V(\lambda/5500\,{\rm Å})^{-0.7} & \text{if } t > t_{\rm MC}, \end{cases} \quad (4)$$

where τ_V indicates the total *V*-band attenuation experienced by young stars within the birth MCs (due to the birth clouds themselves and the diffuse ISM), $t_{\rm MC}$ is the time-scale of destruction of the MC or for stars to migrate out of the birth clouds and μ defines the fraction of the total effective optical depth contributed by the ambient ISM. CF00 used a sample of nearby UV-selected starburst galaxies to test their model and constrain its parameters, by considering the ratio of FIR to UV luminosities, the UV spectral slope and Balmer line ratios (see also Kong et al. 2004). The best-fitting values found by CF00 are $t_{\rm MC} \simeq 10^7$ yr, $\mu \sim 0.3$, with $\tau_V^{\rm ISM} = \mu\,\tau_V \sim 0.5$ and $\tau_V^{\rm MC} = (1-\mu)\,\tau_V \sim 1.0$.

In the spirit of the CF00 model, one can, of course, adopt a composite attenuation curve, e.g. in which the Milky Way extinction curve is used to describe the diffuse 'cirrus' dust, and the CF00 power-law attenuation law is used to describe the situation experienced by young stars in the dense birthclouds. This is the approach taken by DLB07.

3.4 Effective optical depth

Perhaps the most fundamental quantity characterizing the extinction is the *face-on effective optical depth* in a given reference band, usually the *V* band (τ_V). As we discussed in the Introduction, many works have made use of the empirical relation between the intrinsic luminosity in the *B* band and the optical depth (Wang & Heckman

1996). Also very common are variants of the model originally proposed by GRV87, which links the optical depth of the dust at a given wavelength τ_λ to the column density of metals in the cold gas and to τ_V:

$$\tau_\lambda = \left(\frac{A_\lambda}{A_V}\right)\left(\frac{Z_{\rm gas}}{Z_\odot}\right)^s \left(\frac{N_H}{2.1\times10^{21}\,{\rm cm}^{-2}}\right). \quad (5)$$

The exponent s of the metallicity is wavelength dependent: $s = 1.35$ for $\lambda < 2000$ Å, and $s = 1.6$ for $\lambda > 2000$ Å, based on interpolations of the extinction curves of the MW and the Magellanic Clouds. In GRV87, the column density N_H is assumed to be simply proportional to the cold gas fraction:

$$\langle N_H\rangle = 6.8\times10^{21}\frac{M_{\rm gas}}{M_\star + M_{\rm gas}}\,{\rm cm}^{-2}. \quad (6)$$

More recent models, in which an estimate of the radius of the disc has been made available, have used an updated form in which the column density is proportional to the cold gas mass divided by the gas radius squared (e.g. Guiderdoni et al. 1998; Cole et al. 2000; Devriendt & Guiderdoni 2000). DLB07 assume that

$$N_H = \frac{M_{\rm gas}}{1.4 m_p \pi\, r^2}\,{\rm cm}^{-2}, \quad (7)$$

where r is the exponential scale radius of the disc, as predicted by their SAM.

As discussed above, the extinction suffered by young stars enshrouded in dense birth clouds may be greater than that experienced by more evolved stars embedded in more diffuse cirrus. We will adopt the age-dependent extinction prescription proposed by DLB07. They assume that stars younger than $t_{\rm MC}$ (which they take to be 10^7 yr) have an optical depth $\tau_V^{\rm MC} = \tau_V^{\rm cirrus}\,(1/\mu - 1)$, with the value of μ randomly extracted from a Gaussian distribution with $\langle\mu\rangle = 0.3$ and $\sigma_\mu = 0.2$, truncated at 0.1 below and 1.0 above.

3.5 Geometry

The adopted extinction or attenuation curves are then generally combined with simple geometrical configurations having analytical expressions, in order to describe the dependence of the attenuation on the viewing angle i and/or include scattering. The analytical solutions for the RT in simplified geometries are generally taken from Natta & Panagia (1984), Osterbrock (1989), Lucy et al. (1991) and Városi & Dwek (1999).

The simplest and most commonly used assumption is the *slab* configuration, where stars and dust are homogeneously distributed in an infinite plane layer:

$$A_{\lambda,i}^{\rm slab} = -2.5\,\log\left[\frac{1-\exp(-\tau_\lambda/\cos(i))}{\tau_\lambda/\cos(i)}\right]. \quad (8)$$

The τ_λ in the expression is sometimes 'corrected' for scattering by multiplying it by $\sqrt{1-\omega_\lambda}$, where ω_λ is the albedo (GRV87). Other geometries, such as the *oblate ellipsoid*, have also been considered (e.g. Devriendt et al. 1999).

4 RELATING DUST EXTINCTION TO PHYSICAL PARAMETERS

The GRV87 model for the optical depth, and its offshoots, provided a first basic attempt to relate the dust optical depth to physical properties of galaxies such as metallicity and gas column density. As we have discussed, empirically it is also known that dust optical depth correlates with properties such as bolometric or B-band luminosity. Based on RT calculations with the ray-tracing code SUNRISE (Jonsson 2006) applied within hydrodynamical simulations (Cox et al. 2004), Jonsson et al. (2006) found a tight relationship between effective optical depth and combinations of quantities such as metallicity, bolometric luminosity, SFR, stellar mass or baryonic mass. Motivated by these results, we analyse our libraries to attempt to extract a generalized fit for the effective optical depth as a power-law function of these variables, e.g.

$$\tau_V = f(L_{\rm bol}, M_{\rm bar}, {\rm SFR}, Z, M_{\rm gas}, M_\star, r_{\rm gal}). \quad (9)$$

As we discussed in Section 2.2, correlations like the one found by Jonsson et al. (2006) may be in part the result of built-in correlations in the models, e.g. the Schmidt law used in the hydrodynamic simulations relates SFR to gas density. Therefore, we initially explore the dependence of dust obscuration on galaxy properties in our empirical CHE_EVO+GRASIL library, EL, where we have deliberately broken all such built-in correlations. We then explore whether the same correlations hold in the ML.

As we describe in Section 2, in the EL, Z, $M_{\rm gas}$ and SFR are uncorrelated by construction. The remaining four physical quantities ($L_{\rm bol}$, $M_\star$, $M_{\rm bar}$ and $R_{\rm gal}$) follow from the star formation history and our assumed correlation between $M_\star$ and $R_{\rm gal}$. We then perform a fitting procedure to try to recover the 'true' effective optical depth from the GRASIL library, $\tau_V^{\rm GS}$. We computed $\tau_V^{\rm GS}$ from the corresponding face-on GRASIL SEDs. We assume power-law dependences for the values of the seven physical quantities and define general relations involving independent physical quantities. We determine the best-fitting parameters in each relation using a χ^2 minimization technique and repeat the fitting procedure considering the disc-dominated and the bulge-dominated subsamples separately. We start from a relation involving a single physical quantity, and then consider an additional degree of freedom if the resulting reduced χ^2 is lowered by a factor of $\sim$2. Our results show that we usually need to involve at least three physical quantities in order to reproduce $\tau_V^{\rm GS}$ well; and in particular the best-fitting result is obtained by considering the following relation:

$$\tau_V^F = \tau_V^0\left(\frac{Z}{Z_\odot}\right)^\alpha\left(\frac{M_{\rm gas}}{{\rm M}_\odot}\right)^\beta\left(\frac{R_{\rm gal}}{1\,{\rm kpc}}\right)^\gamma. \quad (10)$$

In the following, we refer to the τ_V values predicted by this fitting formula as τ_V^F, and we indicate in parentheses the library we use to calibrate the best-fitting parameters.

The optical depth $\tau_V^{\rm GS}$ in the EL is very clearly related to the gas mass $M_{\rm gas}$, scale radius $R_{\rm gal}$ and Z. This is not surprising, given that the dust-to-gas ratio we have used in GRASIL is proportional to the metallicity (see Section 2.3). However, the relation between $\tau_V^{\rm GS}$ and τ_V^F(EL) shows a large spread for low values of $\tau_V^{\rm GS}$; we checked that this behaviour is connected to low values of the gas surface density $\Sigma_{\rm gas} = M_{\rm gas}/(4\pi R_{\rm gal}^2)$. For this reason, when computing the best-fitting parameters for the EL (see Table 3), we restrict our

Table 3. Best-fitting parameters for equation (10), for the different subsamples. For the CL and ML libraries, the fits are for the combined low- and high-z samples.

	Sample	$\log(\tau_V^0)$	α	β	γ	Scatter (dex)
τ_V^F(EL)	Discs	−4.84	0.39	0.50	−0.99	0.2
	Bulges	−3.63	0.43	0.34	−0.65	0.2
τ_V^F(CL)	Discs	−5.59	0.27	0.56	−1.05	0.1
	Bulges	−6.47	0.21	0.65	−1.03	0.5
τ_V^F(ML)	Disc-Dom.	−5.50	0.19	0.55	−0.98	0.1
	Bulge-Dom.	−5.77	0.32	0.58	−0.79	0.4

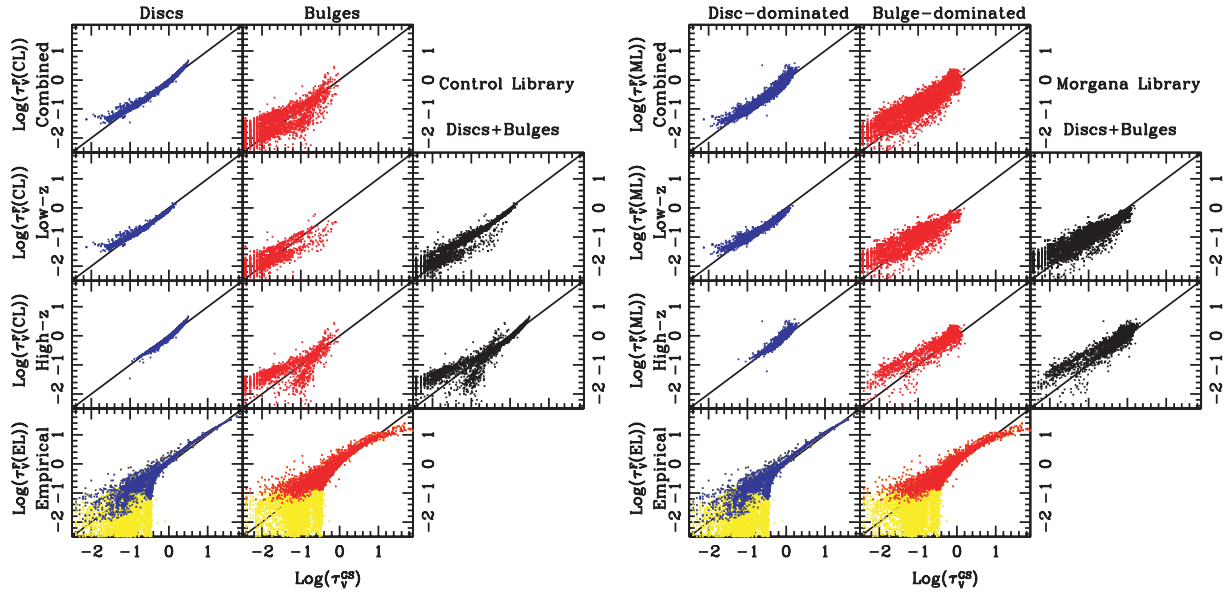

Figure 2. Comparison between the 'true' optical depth from the RT libraries $\tau_V^{\rm GS}$ and the predictions of our best-fitting formulae (equation 10). The bottom row shows the results from the EL. The upper three rows show the results from the combined (high-z plus low-z), and separate high- and low-z samples (as labelled) for the CL (left-hand plot) and the ML (right-hand plot). Vertical columns within each plot show the bulge-dominated, disc-dominated, and combined (bulge and disc) samples, as labelled.

analysis to objects with $\Sigma_{\rm gas} > 1\,{\rm M}_\odot\,{\rm pc}^{-2}$ for the EL discs and $\Sigma_{\rm gas} > 100\,{\rm M}_\odot\,{\rm pc}^{-2}$ for the EL bulges (the different values are related to the different meaning of the scale radius in the two geometries). The best-fitting relation between $\tau_V^{\rm GS}$ and τ_V^F(EL) is shown in Fig. 2 (lower panels). Yellow dots refer to the whole EL, whereas blue and red dots refer to the objects with a gas surface density higher than the threshold.

We then consider the SEDs in the CL. Recall that the CL uses the star formation and enrichment histories predicted by MORGANA, but with bulge-dominated systems represented by a pure bulge and disc-dominated systems represented by a pure disc. We see that τ_V^F(EL) provides a good approximation for $\tau_V^{\rm GS}$ in this library, for the disc sample. On the other hand, most of the objects with bulge geometry lie below our surface density threshold, and therefore τ_V^F(EL) is not a good solution for this subsample: in particular, it provides a systematic underestimate of the $\tau_V^{\rm GS}$. We then redetermine the best-fitting parameters for equation (10) (i.e. the relation involving $M_{\rm gas}$, $R_{\rm gal}$ and Z) on the combined (low z + high z) CL and collect the results in Table 3. In Fig. 2 (left-hand panel), we show the comparison between $\tau_V^{\rm GS}$ and τ_V^F(CL): for the pure discs the fit is accurate both for the combined and for the two separate samples; for the pure bulges, the quality of the fit is slightly different for the 'low-z' and 'high-z' samples.

When we include the effect of complex geometry in the ML, both τ_V^F(EL) and τ_V^F(CL) do not correctly reproduce $\tau_V^{\rm GS}$. The CL fit parameters still provide a good approximation for the intrinsic optical depth for the bulge-dominated subsamples. However, the presence of a bulge perturbs the SED of the disc-dominated objects. The effect grows when massive bulges are considered, and it is larger if the bulge component is actively forming stars. These effects are more important for the high-z galaxies, where both conditions are frequent in MORGANA. Again, we re-calibrate the best-fitting parameters for equation (10) on the combined (low z + high z) ML, and collect our results in Table 3. We then compare τ_V^F(ML) and $\tau_V^{\rm GS}$ in Fig. 2 (right-hand panel). The figure shows that we obtain a reasonable fit to the combined sample, with a scatter of 0.1 and 0.4 dex for the disc and bulge samples, respectively. However, several problems arise when we consider the separate samples. We first discuss the disc-dominated subsamples, where we find an overestimate at the level of $\sim$1 dex for the high-z sample. This is due to objects with a significant bulge component (in mass, star formation activity or both). On the other hand, when applied to the bulge-dominated subsamples, τ_V^F(ML) provides a systematic overestimate of $\tau_V^{\rm GS}$ for the high-z sample and a systematic underestimate for the low-z sample, both at the level of 0.5 dex.

The fitting formula we propose in equation (10) is analogous to standard analytic prescriptions, for example the GRV87 and DLB07 approaches. However, it is interesting that the best-fitting values for the parameters δ, ϵ and η differ from the equivalent values generally used in the literature. Not too surprisingly, the combination of best-fitting parameters for $M_{\rm gas}$ and $R_{\rm gal}$ hints of a dependence of $\tau_V^{\rm GS}$ on the cold gas surface density (for all fits in Table 3, $\gamma \sim 2\,\beta$). This is similar to equation (7), even if in the latter equation the dependence is linear with the cold gas surface density. The dependence of $\tau_V^{\rm GS}$ on metallicity Z is completely different, and much weaker than in equation (5).

5 COMPARISONS AT OPTICAL WAVELENGTHS

In this section, we compare the results of the GRASIL libraries with several approximations. In all of these approximations, we assume that the wavelength and geometry-dependent behaviour of the dust extinction can be captured by using an expression that relates the effective optical depth τ_V to physical properties of the galaxy, in combination with a 'slab' model for the geometry and the DLB07 composite MW + CF00 attenuation curve (see Section 3; following DLB07, we select μ randomly from a Gaussian distribution). We assume a single dust slab to describe the attenuation of both disc and bulge. To assure proper comparison with the GRASIL SEDs, we

Table 4. Dust prescriptions.

Prescription	Optical depth
TAU-GS	'True' optical depth from GRASIL (τ_V^{GS})
TAU-FIT	Results of fit to GRASIL libraries (τ_V^F(ML))
TAU-GRV	Guiderdoni & Rocca-Volmerange (1987; GRV87)
TAU-DLB	De Lucia & Blaizot (2007; DLB07)

also average slab model results over inclination. We will refer to the four prescriptions that we will test as:

(i) Prescription TAU-GS: we use the actual value of the effective optical depth τ_V^{GS} from the RT library.
(ii) Prescription TAU-FIT: we use the fitting formula τ_V^F(ML) derived in Section 4.
(iii) Prescription TAU-GRV: we use the GRV87 formula (equation 5) for τ_V. Recall that in this approximation, the column density of the gas is simply proportional to the gas fraction (no scaling with galaxy radius).
(iv) Prescription TAU-DLB: we use the DLB07 formula (equation 7) for τ_V. Here, the optical depth is proportional to the surface density of the gas (scales as $1/r_{gal}^2$).

These prescriptions are summarized in Table 4.

We have extensively tested many different possible combinations of ingredients, for example, substituting the Calzetti or CF00 attenuation law for the Galactic extinction law, or substituting the oblate ellipsoid geometry for the slab model. We find a similar level of agreement with the Calzetti law, but worse agreement with the CF00 attenuation law. The oblate ellipsoid geometry produces similar results to the slab model.

5.1 Attenuation curves

In Fig. 3 (left-hand panel), we show the V-band normalized attenuation curves A_λ^{GS} for the GRASIL SEDs in the ML. The yellow shaded area is for the low-z sample and the diagonal texture for the high-z sample (1σ confidence regions). It is worth noting that the galaxy-to-galaxy scatter shown in Fig. 3 is an underestimate, as we do not consider the distribution of inclination angles (but only angle-averaged SEDs) and we keep fixed both t_{esc} and the intrinsic properties of dust grains. For comparison we also display the average MW extinction curve (by Mathis et al. 1983, dotted red line), and the attenuation curves of Calzetti et al. (2000) (dashed blue line), CF00 (dot–dashed green line), and the slab + MW extinction + scattering (continuous red line). All curves have been normalized to $\tau_V = 1$ in order to highlight the different dependencies on the wavelength.

The comparison with the Calzetti et al. curve is particularly interesting, since its shape has been interpreted in several ways. For instance, Gordon et al. (1997) ascribed the observed shape to the presence of dust lacking the 2175 Å feature in the extinction curve, i.e. intrinsic dust differences. This interpretation is probably a consequence of adopting a model that accounts for the clumping of dust but not of stars, and with a spatial distribution of stars independent of stellar age. Granato et al. (2000) reproduced this featureless and shallow attenuation as a result of the complex and wavelength-dependent geometry where the UV-emitting stars are heavily embedded inside MCs, while older stars, mainly emitting in the optical and NIR, suffer a smaller effect from the diffuse medium. Similar conclusions on the strong effect of complex geometries in the resulting attenuation have been found in the analysis by e.g. Panuzzo et al. (2003, 2007), Pierini et al. (2004), Tuffs et al. (2004), Inoue (2005) and Inoue et al. (2006). While one can be confident that intrinsic dust differences are effectively present in different galaxies, as well as in different environments, it also appears that the complex geometry in galaxies can have a major and sometimes dominant role.

Since, as described in Section 2.3, in the MORGANA+GRASIL models the dust properties (size distribution and composition) are fixed so as to reproduce the average MW *extinction* curve, any difference between that and the *attenuation* curves we obtain must be ascribed to the particular geometrical configuration of each model galaxy. As

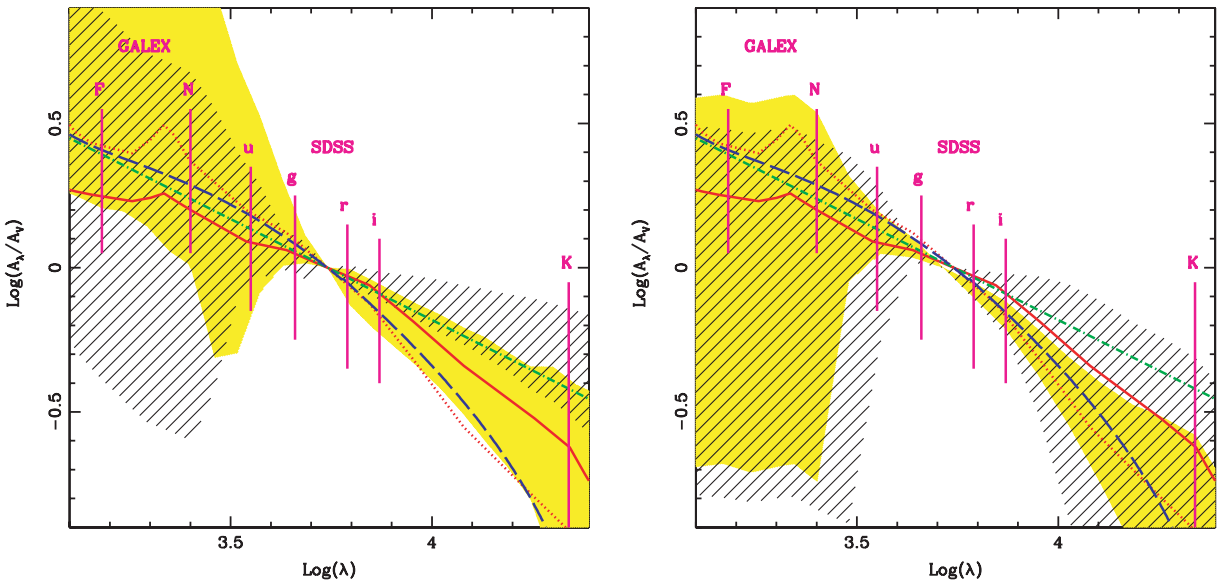

Figure 3. Left-hand panel: the V-band normalized attenuation curves obtained by MORGANA+GRASIL for the low- and high-z samples (yellow shaded area and diagonal texture, respectively) are shown compared with the MW extinction law (dotted red line, by Mathis et al. 1983), Calzetti et al. (dashed blue line), CF00 (dot–dashed green line) and the *slab* + with the MW extinction (continuous red line) attenuation curves. Right-hand panel: the same quantities for Prescription TAU-GS (see Section 5.2).

we said, the geometry has to be understood in a broad sense, i.e. not only the stars and dust distributions in a bulge and/or in a disc, but also the clumping of stars and dust and the age-dependence, therefore wavelength-dependence, of the amount of attenuation suffered by stars. We stress that the attenuation curve we obtain for each model would be exactly equal to the adopted extinction curve if we were to assume that all the dust is in a foreground screen in front of the stars and no scattered light reached the observer. Therefore, the very large spread we get, as evident from the figure, has to be ascribed to the accounting of the star formation histories, the distribution of stars and dust with the appropriate radii and the connection between stellar populations of different ages with different dusty environments.

We also show in Fig. 3 (right-hand panel) the corresponding mean attenuation as a function of wavelength for Prescription TAU-GS; i.e. using the composite attenuation law suggested by DLB07 based on the CF00 model. Encouragingly, the behaviour is qualitatively similar to that of the intrinsic GRASIL mean attenuation curve. The major discrepancies arise at very short wavelengths (in both samples), where GRASIL predicts larger attenuations, and in the NIR region (in the high-z sample), where GRASIL predicts a smaller scatter and on average larger attenuations. We test that the scatter in the attenuation laws at short wavelengths is reduced if we assume a fixed value for the μ parameter (i.e. $\mu = 0.3$) in Prescription TAU-GS, instead of using a Gaussian distribution.

5.2 Attenuation and colour excess

In this section, we show the results we obtain for attenuation and reddening by coupling MORGANA either with the full GRASIL RT calculation or by applying different prescriptions for attenuation to the pure stellar SED (summarized in Table 4). We illustrate our comparison by showing attenuations and colour excesses as a function of $M_\star$ and specific star formation rate $r_{\rm SFR}$. We show the results for the *FUV* GALEX filter, the g and r SDSS filters and the K-band bandpass, but similar results hold if we consider the full set of SDSS bandpasses plus NIR photometry. We also consider bulge- and disc-dominated subsamples separately. We consider rest-frame magnitudes both for the low-z and for high-z samples. This choice allows us to test the robustness of different prescription for dust attenuation, when changing the properties of the underlying galactic populations.

In Fig. 4, we compare $E^{\rm GS}(g-r)$, $E^{\rm GS}(r-K)$, $A^{\rm GS}_{\rm FUV}$ and $A^{\rm GS}_g$ to the corresponding quantities obtained when $\tau_V^{\rm GS}$ is combined with a composite attenuation law like DLB07 (Prescription TAU-GS; shaded areas and diagonal texture represent the 1σ confidence regions). Clearly, this case provides a reference point for whole analytic approach – in principle, none of our other prescriptions can possibly do better at reproducing the full GRASIL results than this one, where the effective optical depth is measured directly from the RT libraries.

Indeed, we see that this model provides a satisfactory representation of the RT results at optical wavelengths. Mean attenuations are slightly underpredicted, but the trends as a function of $M_\star$ and $r_{\rm SFR}$ are correctly recovered. However, the agreement worsens at shorter wavelengths, with a significant underprediction of the level of attenuation. This result is expected: at FUV wavelenghts the attenuation is extremely sensitive to the details of the dust distribution and composition, and it is very difficult to describe it with a simple analytic formulation. This result can also be understood in terms of the different distributions of attenuation that we have already seen in Fig. 3. The same prescription is able to reproduce $A^{\rm GS}_{\rm FUV}$ and $A^{\rm GS}_g$ for the high-z sample, but the agreement is poor for both colour excesses, particularly in the disc-dominated sub-sample. Again, this reflects the disagreement in the attenuation curves.

We compare the same quantities for our TAU-FIT prescription in Fig. 5. The agreement is again satisfactory, and more importantly where there are discrepancies, they are similar to those seen in Prescription TAU-GS. This indicates that the main source of remaining error is not our fitting results for τ_V but rather the simplified approach we have used to estimate the attenuation curve.

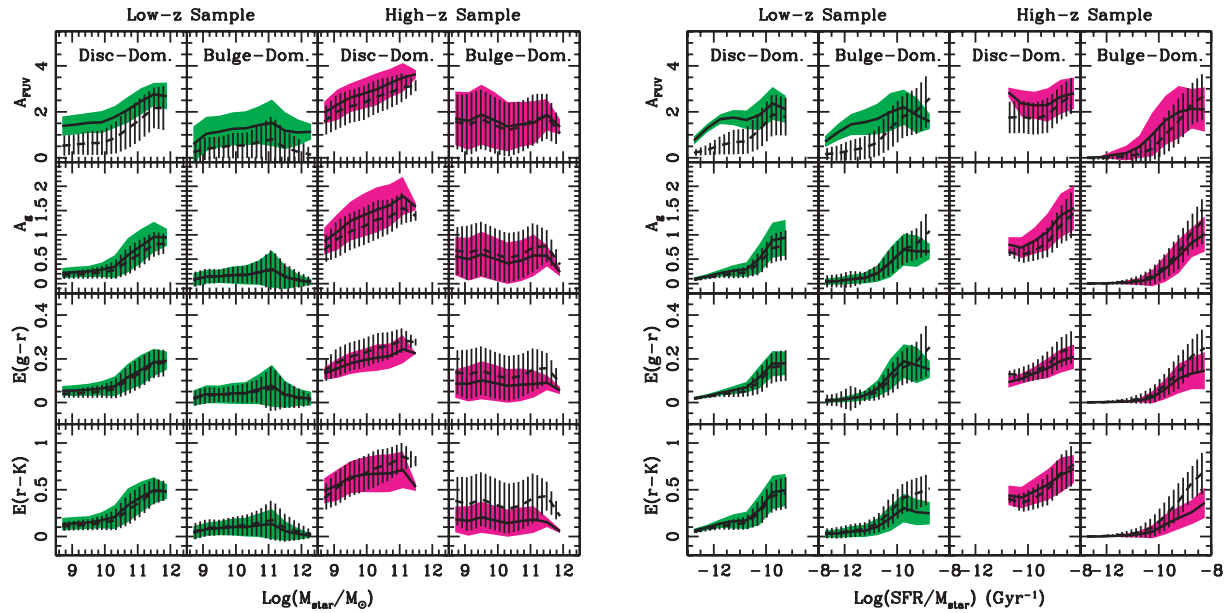

Figure 4. Comparison between the colour excesses $E^{\rm GS}(g-r)$ and $E^{\rm GS}(r-K)$, and the attenuations $A^{\rm GS}_{\rm FUV}$ and $A^{\rm GS}_g$ (shaded areas) as a function of stellar mass $M_\star$ (left-hand panel) and of specific SFR (right-hand panel), with the predictions of Prescription TAU-GS (vertical texture). We show the results separately for the disc- and bulge-dominated samples and for the low- and high-z samples, as labelled in the figure.

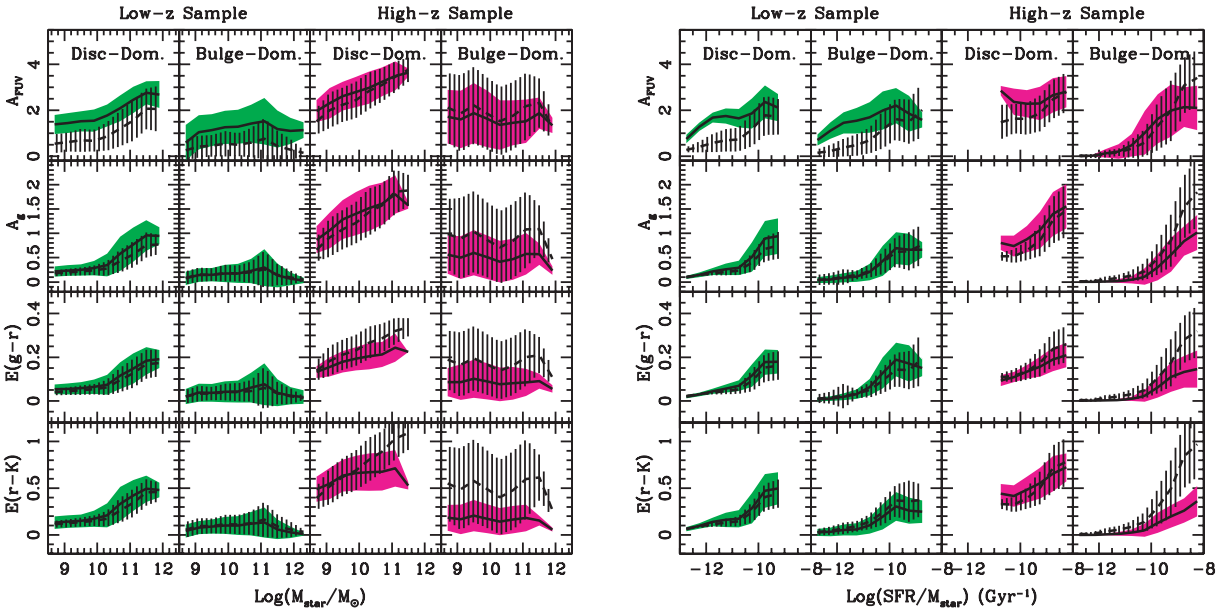

Figure 5. Same as in Fig. 4. The vertical textured area shows the predictions of Prescription TAU-FIT.

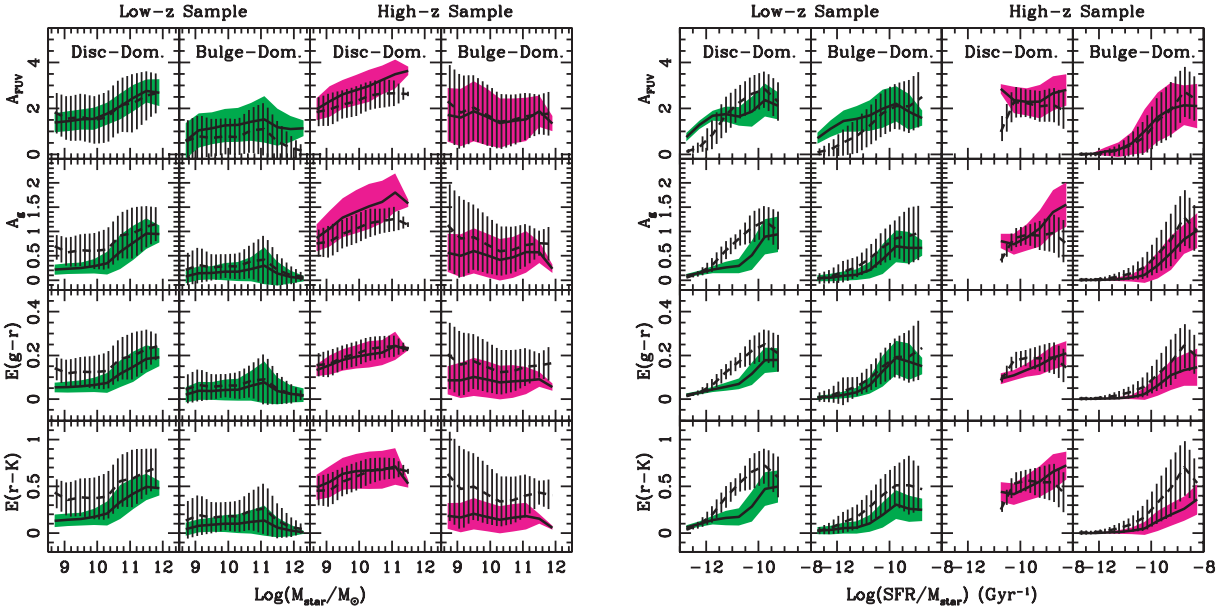

Figure 6. Same as in Fig. 4. The vertical textured area shows the predictions of Prescription TAU-GRV.

We show in Fig. 6 the same comparison with Prescription TAU-GRV. In the low-z sample (left-hand panel), the ranges covered by the model and the prescription are in reasonable agreement, despite a slight systematic overestimate of attenuation and colour excess in both the disc-dominated and the bulge-dominated sample. The dependence of attenuation on $M_\star$ is at least approximately reproduced. The dependence of attenuation and colour excess on $M_\star$ is only marginally reproduced, with a larger discrepancy for the bulge-dominated objects. Moreover, the distributions of attenuations and colour excesses around the mean values show a smaller (larger) scatter with respect to GRASIL predictions for disc-(bulge-) dominated objects. The effect of considering a simple geometry is similar to the low-z case (higher attenuations and colour excesses for the pure discs and vice versa for the pure bulges).

Finally, we show in Fig. 7 the comparison with Prescription TAU-DLB. Following the original work, for each object we compute $r_{1/2}$ starting from the disc scale radius (even if the galaxy is bulge-dominated). Prescription TAU-DLB is able to reproduce both GRASIL attenuations and colour excesses and their dependence on $M_\star$ in the low-z sample, with the notable exception of the far-UV attenuations. Moreover, the scatter is always larger than the corresponding quantity in GRASIL. Quite interestingly, a very similar behaviour is obtained for the CL, with only small differences with respect to the ML. We then conclude that Prescription

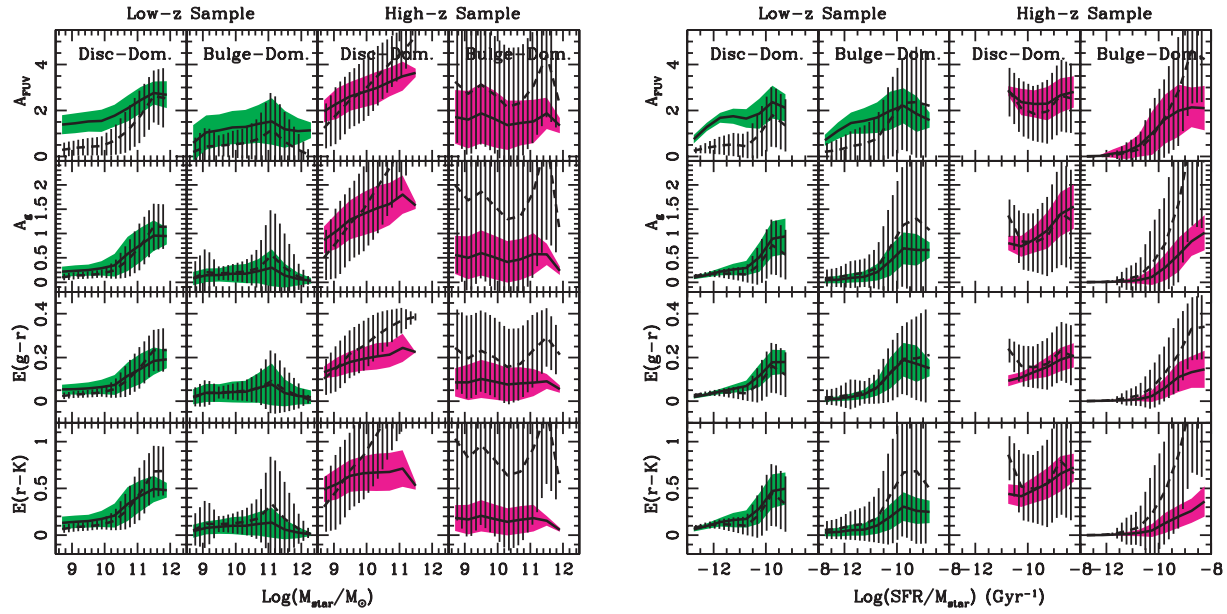

Figure 7. Same as in Fig. 4. The vertical textured area shows the predictions of Prescription TAU-DLB.

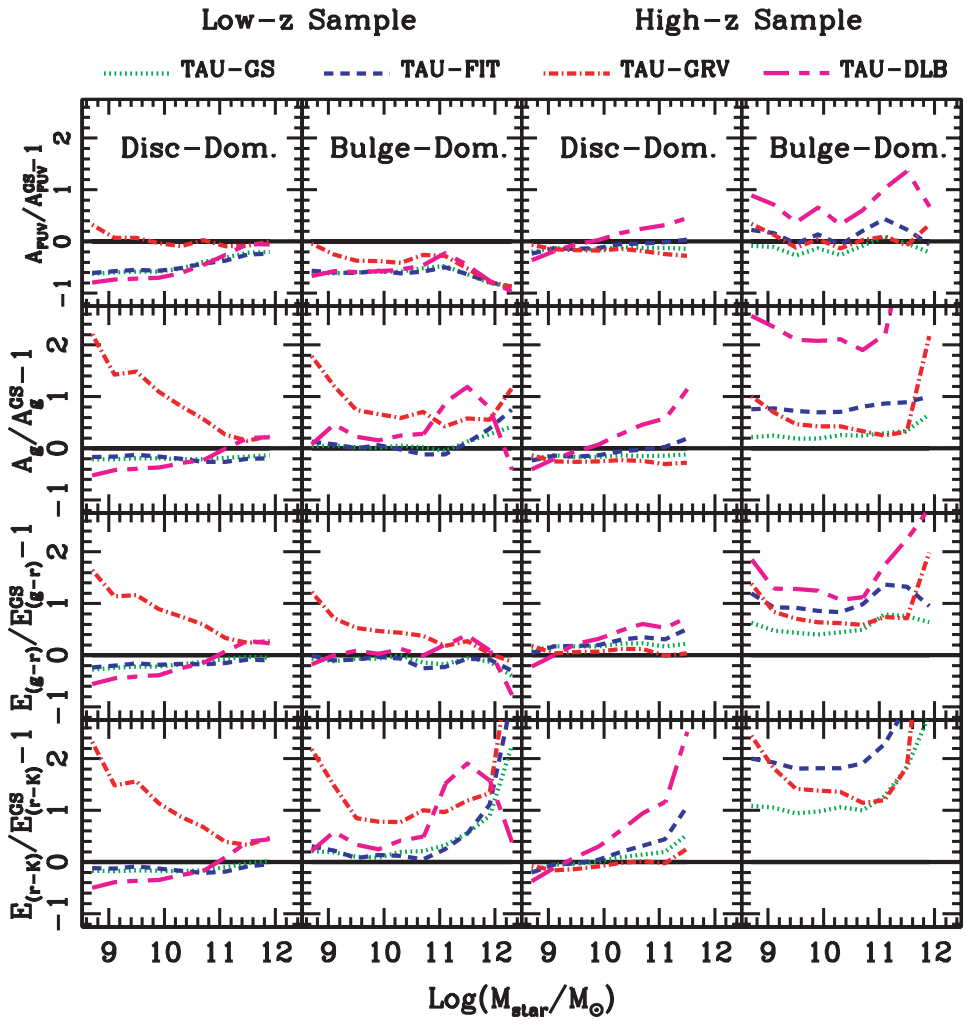

Figure 8. Residuals in the mean attenuations as a function of stellar mass for our four prescriptions with respect to GRASIL predictions. Dotted, dashed, dot–dashed, long–short dashed lines refer to prescription TAU-GS, TAU-FIT, TAU-GRV and TAU-DLB, respectively.

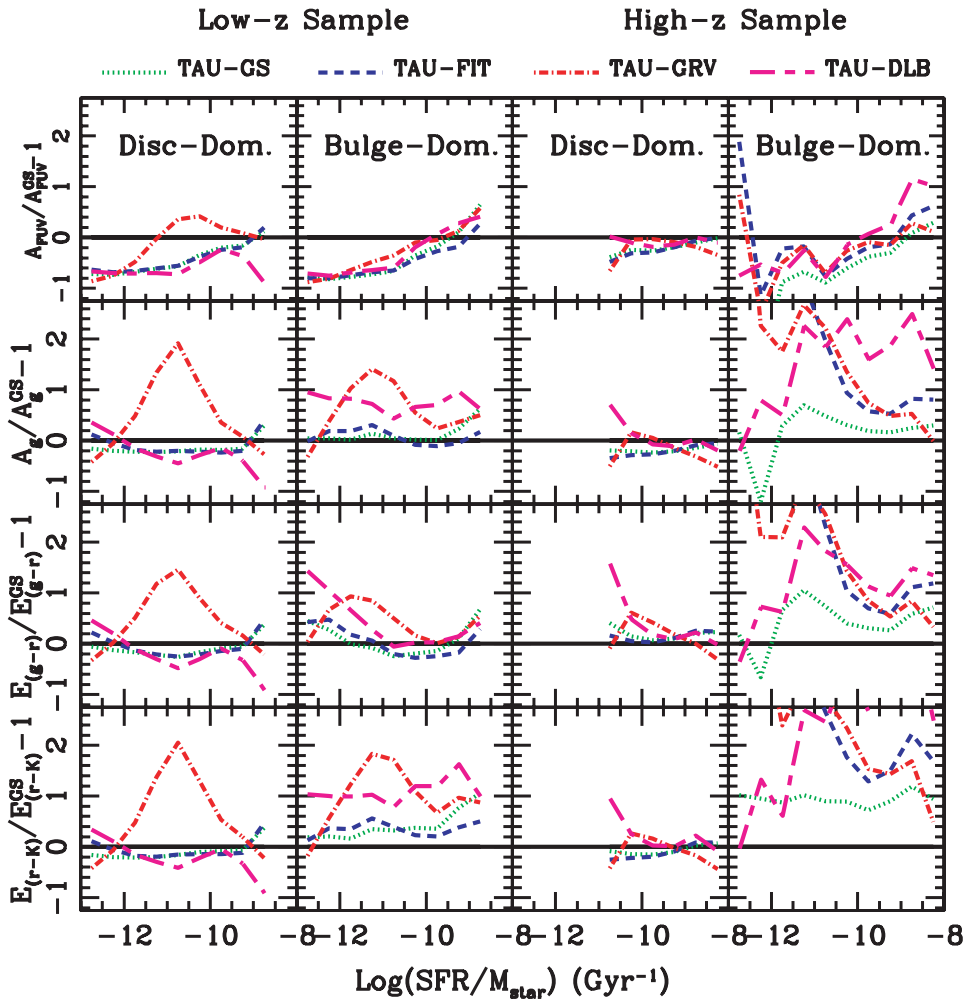

Figure 9. Residuals in the mean attenuations as a function of specific SFR for our four prescriptions with respect to GRASIL predictions. Lines are as in Fig. 8.

TAU-DLB is less sensitive to the composite versus simple geometry than Prescription TAU-GRV. On the other hand, when we compare Prescription TAU-DLB to the high-z sample, we obtain both a steeper dependence of attenuation from $M_\star$ and a larger scatter with respect to GRASIL.

Both Prescriptions TAU-GRV and TAU-DLB provide acceptable agreement with the GRASIL results for the low-z samples, but they do not do well at high redshift. The satisfactory agreement at low z is not surprising, given the fact that the original prescriptions are calibrated to reproduce the properties of galaxies in the local Universe. The origin of the high-z discrepancy lies in the different distribution of cold gas fractions and surface densities in the two samples (the dependence on Z and $M_{\rm gas}$ being the same). The DLB07 prescription for τ_V is proportional to the gas surface density; we demonstrate that this assumption is broadly consistent with the RT results; however our analysis suggests a much weaker dependence of τ_V on surface density (to the square-root power). We therefore expect the differences to grow at high z, where gas surface densities are considerably higher.

From Figs 8 to 11, we summarize the results for all four prescriptions in terms of the residuals of the difference between the mean attenuation predicted by the prescription and the intrinsic attenuation in GRASIL. From these figures, we can clearly see that prescription TAU-GS always has the smallest residuals, as expected. Prescription TAU-FIT is seen to be quite successful in that in most cases, the residuals are similar to those of prescription TAU-GS and the trends are similar. Prescriptions TAU-GRV and TAU-DLB show a similar level of agreement overall, but often show different trends with galaxy properties such as stellar mass. All prescriptions seem to have particular difficulty reproducing the GRASIL results for high-z bulge-dominated galaxies.

Finally, we assess the impact of the different dust prescriptions on the predictions of the statistical properties of galactic samples. In particular, in Fig. 12 we focus on the resulting luminosity functions, which are commonly used as a baseline prediction for SAMs. The thin solid line represents the unextinguished luminosity function at different wavelengths for the low- and high-z samples, whereas the thick solid line shows the luminosity function of the samples as predicted by GRASIL. The other lines represent Prescription TAU-GS, TAU-FIT, TAU-GRV and TAU-DLB (the dotted, dashed, dot–dashed and long–short dashed line, respectively). This comparison is quite encouraging, in that it indicates that, while it is extremely important to correct for the effects of dust, particularly at high redshift and in shorter wavelength bands, even a simple analytic approach gives quite good results, when dealing with integrated quantities, such as the LFs, in which galaxy-to-galaxy differences are smoothed out, particularly in the optical-NIR region characterized by relatively regular and featureless SEDs. However, the spread

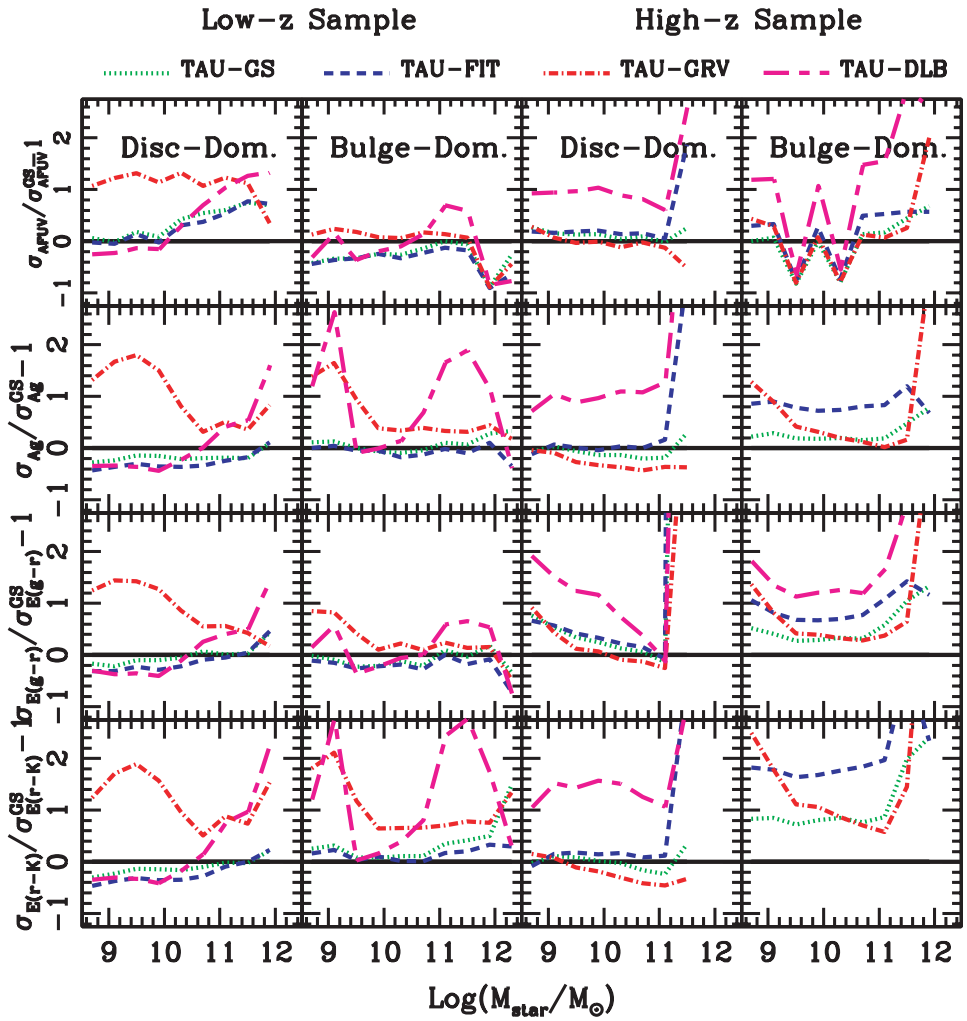

Figure 10. Residuals in the variance in the mean attenuations as a function of stellar mass for our four prescriptions with respect to GRASIL predictions. Lines are as in Fig. 8.

in the predicted LF increases at UV wavelengths. As we have seen, the effect of dust on galaxy colours is not reproduced as well by the simple analytic prescriptions.

5.3 Inclination dependence of attenuation

The geometrical dependence of the predicted SEDs manifests itself also in the dependence of attenuation on the viewing angle. In many papers, statistical estimates of the dust opacity in galaxy discs have been worked out, through the analysis of the inclination dependence of apparent magnitudes and colours of large samples of spiral galaxies (e.g. de Vaucouleurs et al. 1991; Giovanelli et al. 1995; Moriondo, Giovanelli & Haynes 1998; Tully et al. 1998; Graham 2001; Masters, Giovanelli & Haynes 2003). Extensive work on the angle dependence predicted by RT models (chiefly for disc galaxies) has also been presented in the literature (e.g. Kylafis & Bahcall 1987; Byun, Freeman & Kylafis 1994; Bianchi, Ferrara & Giovanardi 1996; Kuchinski et al. 1998; Tuffs et al. 2004; Pierini et al. 2004; Rocha et al. 2008). The interpretation of observations to infer opacities, scalelengths, luminosities, etc. is non-trivial, because of the radial gradients in the dust distribution and metallicity thus in the dust opacity, the different scaleheights of stars and dust, the bulge to disc ratio, and the inclination effects (e.g. Xilouris et al. 1999; Boissier et al. 2004; Popescu et al. 2005; Möllenhoff, Popescu & Tuffs 2006; Driver et al. 2007).

The statistical data for the attenuation–inclination dependence may therefore provide a further test for SAM predictions (see e.g. Granato et al. 2000), if the spectral properties computed for the SAM are reliable, given the complexities described above. In the previous sections, we have considered the results we obtain for angle-averaged SEDs. In Fig. 13, we show the dust net attenuation (difference edge-on to face-on) predicted using GRASIL and Prescription TAU-DLB, which we recall adopts an infinite plane-parallel *slab* (equation 8). It is evident that the predicted net attenuations are very different in the two cases. We do not want to discuss here the agreement of the result with respect to data, we only wish to point out with one example the clearly different behaviour in terms of both trend and spread. Part of the difference is surely due to the fact that with a slab the net attenuation is independent of the bulge-to-disc ratio given by the SAM. Instead, as discussed by Tuffs et al. (2004), Pierini et al. (2004) and Driver et al. (2007), the attenuation suffered by a dustless bulge seen through the disc can be very pronounced as a function of the viewing angle, depending on the scale radii of stars and dust. In MORGANA, most bulges host relevant star formation activity within dusty MCs, therefore in these cases the total effective attenuation of the galaxy is dominated by

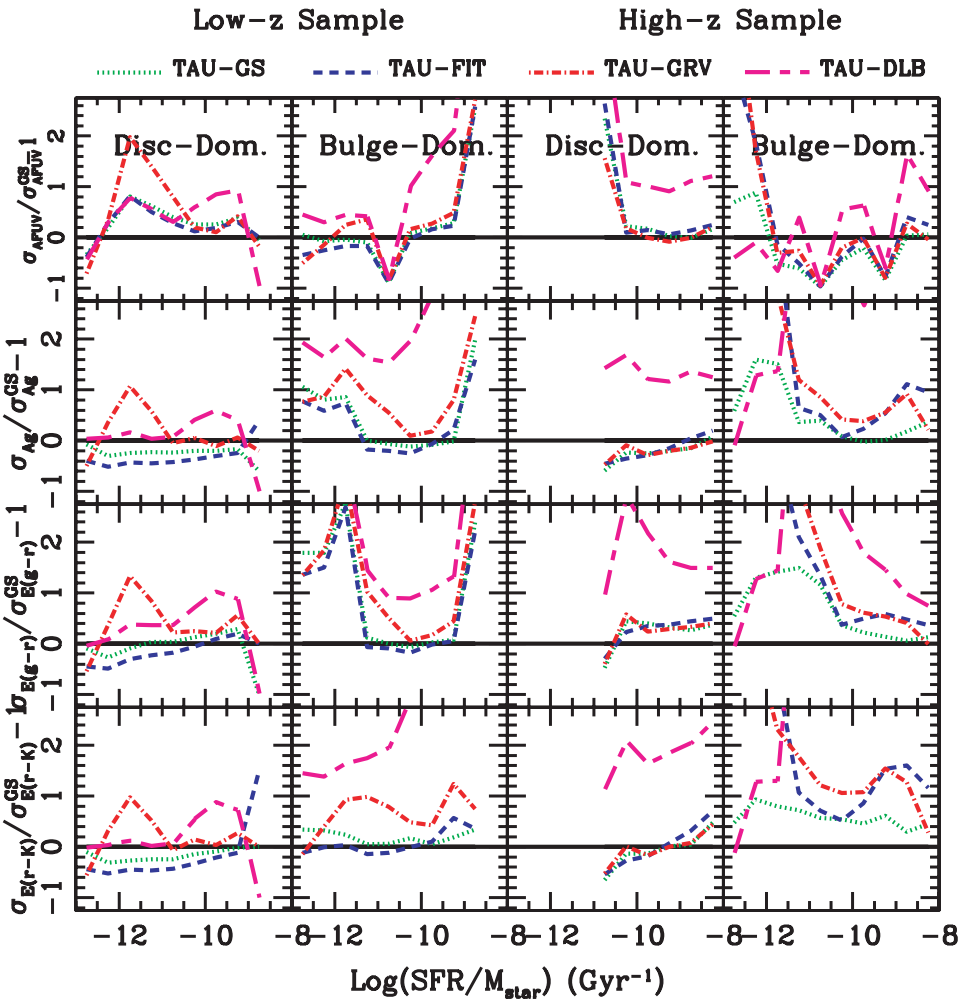

Figure 11. Residuals in the variance in the mean attenuations as a function of specific SFR for our four prescriptions with respect to GRASIL predictions. Lines are as in Fig. 8.

(spherically symmetric) bulges rather than by discs, and this results in lower values and spread of the net attenuation as compared to a slab distribution.

6 SUMMARY

In this paper, we attempt to better understand and quantify the results of detailed RT and dust models (GRASIL), with the goal of assessing and improving the treatment of dust in SAMs of galaxy formation. We build several different libraries of star formation/chemical enrichment histories, which we couple with the GRASIL RT code. One library is based on the MORGANA SAM, with galaxies extracted from two different redshift intervals ($z < 0.20$ and $2 < z < 3$). As a first choice, we keep the composite geometry (bulge+disc) predicted by the SAM; we additionally define a CL by considering only the dominant galactic component (bulge or disc). We then build a third library using the chemical evolution code CHE_EVO and requiring that cold gas mass, metallicity and SFR are both independent and uniformly distributed in the (SFR, $M_{\rm gas}$, Z) space. For this EL, we consider a simpler geometry (pure bulge or pure disc). We then interface the star formation histories with the spectrophotometric code GRASIL to obtain the corresponding synthetic extinguished and unextinguished SEDs.

We compute the intrinsic optical depth in the V-band $\tau_V^{\rm GS}$ for each object, and we combine this estimate with different prescriptions for the attenuation law and for the relative geometry of stars and dust. We find that the GRASIL results are best reproduced by a composite attenuation law as proposed by DLB07, which consists of a power law in wavelength for the young stellar population, as suggested by CF00, and a Galactic extinction curve plus a slab model for older stars. However, we note that even a simpler model with a Galactic extinction law plus a slab model is already a good approximation for the GRASIL results, if the 'true' value of $\tau_V^{\rm GS}$ is known.

We then try to estimate the dependence of $\tau_V^{\rm GS}$ on physical properties of the model galaxies in the EL. We find that $\tau_V^{\rm GS}$ depends mostly on the gas metallicity, on the cold gas mass and on the radius of the system. We provide fitting formulae that are able to predict $\tau_V^{\rm GS}$ over a large dynamical range and with reasonable scatter. We then compare the predictions of the fitting formulae with the intrinsic optical depth for SAM model galaxies. We find that the proposed fitting formulae are able to provide a reasonable fit to $\tau_V^{\rm GS}$ in both redshift intervals. The proposed fitting formulae are analogous to the GRV87 and DLB07 prescriptions; however, we find different power-law dependencies with respect to those models.

We compare the GRASIL attenuations with prescriptions combining the DLB07 composite attenuation law with different estimates of

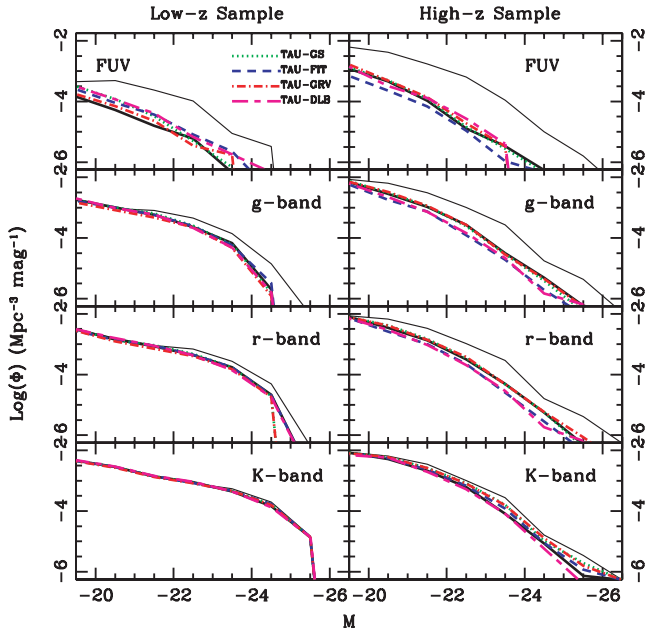

Figure 12. Effect of the different prescriptions for dust absorption on the galaxy luminosity function in different bands. Lines are as in Fig. 8. Thin solid line refers to the unextinguished luminosity function.

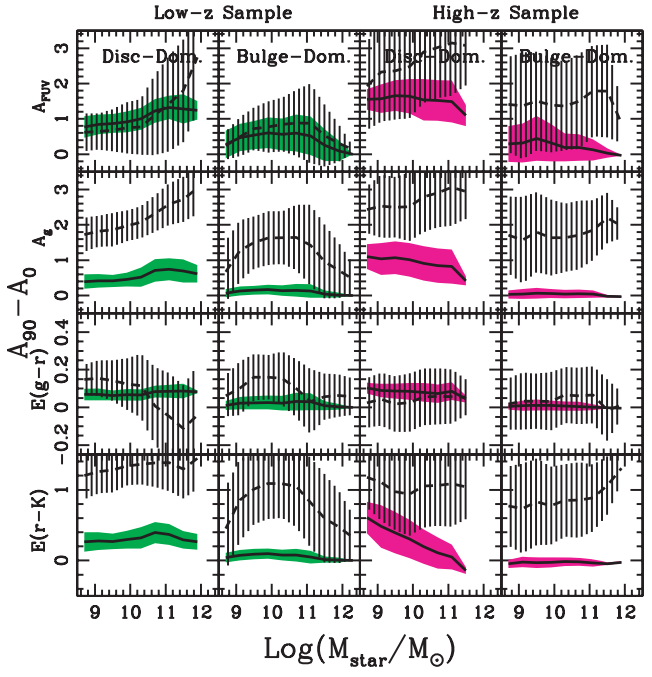

Figure 13. Edge-on relative to face-on attenuation, $A_{90} - A_0$, as a function of stellar mass. The shaded area shows the GRASIL results and the vertical texture the prediction of Prescription TAU-DLB.

τ_V. We conclude that our new fitting formula is able to reproduce the distribution of attenuations and their scaling with galaxy properties, such as stellar mass and specific SFR, nearly as well as the model that uses the actual value of τ_V^{GS} extracted from the RT libraries. The analytic recipes from the literature (GRV87; De Lucia & Blaizot 2007) do reasonably well at low z but give poor results at high z.

It is important to keep in mind that the SAM can provide many physical properties of galaxies to GRASIL, such as SFR, gas density and metallicity, and disc and bulge sizes, but it cannot provide many important physical quantities of the ISM, like the fraction of gas in MCs, the time-scale after which massive stars emerge from the heavily obscuring MCs or the distribution of grain sizes. For the sake of simplicity, we have kept the values of these parameters fixed for all model galaxies in our libraries. Our choice reflects a parameter combination that has been proven adequate for reproducing the properties of $z < 3$ galaxies (Silva et al. 1998; Fontanot et al. 2007). Little is known about the redshift evolution of dust grain properties: a strong systematic variation of these parameters may indeed affect the validity of our fitting formulae. Observations of dust properties in the host galaxies of high-z quasars (see e.g. Maiolino et al. 2004) suggest that the intrinsic properties of dust grains (i.e. composition and dimension) are indeed likely to change at $z > 4$. This is probably due to the fact that at such redshifts dust is mainly produced by Type II supernovae, whereas at lower redshift the contribution from the envelopes of evolved low-mass stars becomes dominant. Therefore, we conclude that our fitting formulae may be limited by this effect to $z < 3$. Finally, it is worth noting that even neglecting any variation of dust properties with redshift, we still find a large dispersion in the resulting attenuation laws: this result suggests that the effect of the geometry and the complexity of star formation histories dominate over the properties of the dust grains (see e.g. Granato et al. 2000).

Our results show that the use of a spectro-photometric code coupled with a simple attenuation law may introduce a systematic shift in the predicted magnitudes. This effect has to be taken into account as an uncertainty associated with models when comparing their prediction to observations. The best way to decrease this systematic error is to use a full RT computation.

ACKNOWLEDGMENTS

The authors would like to thank Gabriella De Lucia for many enlightening and detailed explanations of their model, and Patrick Jonsson, Richard Tuffs and Cristina Popescu for stimulating discussions. Some of the calculations were carried out on the PIA cluster of the Max-Planck-Institut für Astronomie at the Rechenzentrum Garching.

REFERENCES

Babbedge T. S. R. et al., 2006, MNRAS, 370, 1159
Baugh C. M., 2006, Rep. Prog. Phys., 69, 3101
Baugh C. M., Lacey C. G., Frenk C. S., Granato G. L., Silva L., Bressan A., Benson A. J., Cole S., 2005, MNRAS, 356, 1191
Bell E. F., Baugh C. M., Cole S., Frenk C. S., Lacey C. G., 2003, MNRAS, 343, 367
Bianchi S., Ferrara A., Giovanardi C., 1996, ApJ, 465, 127
Blaizot J., Guiderdoni B., Devriendt J. E. G., Bouchet F. R., Hatton S. J., Stoehr F., 2004, MNRAS, 352, 571
Boissier S., Boselli A., Buat V., Donas J., Milliard B., 2004, A&A, 424, 465
Bressan A., Granato G. L., Silva L., 1998, A&A, 332, 135
Bressan A., Silva L., Granato G. L., 2002, A&A, 392, 377
Brinchmann J., Charlot S., White S. D. M., Tremonti C., Kauffmann G., Heckman T., Brinkmann J., 2004, MNRAS, 351, 115
Bruzual G., Charlot S., 2003, MNRAS, 344, 1000
Bruzual A. G., Magris G., Calvet N., 1988, ApJ, 333, 673
Burgarella D., Le Floc'h E., Takeuchi T. T., Huang J. S., Buat V., Rieke G. H., Tyler K. D., 2007, MNRAS, 380, 986
Byun Y. I., Freeman K. C., Kylafis N. D., 1994, ApJ, 432, 114
Calzetti D., 2001, PASP, 113, 1449

Calzetti D., Kinney A. L., Storchi-Bergmann T., 1994, ApJ, 492, 582
Calzetti D., Armus L., Bohlin R. C., Kinney A. L., Koorneff J., Storchi-Bergmann T., 2000, ApJ, 533, 682
Cardelli J. A., Clayton G. C., Mathis J. S., 1989, ApJ, 345, 245
Chapman S. C., Blain A. W., Smail I. R., Ivison R. J., 2005, ApJ, 622, 772
Charlot S., Fall S. M., 2000, ApJ, 539, 718 (CF00)
Cole S., Lacey C. G., Baugh C. M., Frenk C. S., 2000, MNRAS, 319, 168
Cox T. J., Primack J., Jonsson P., Somerville R. S., 2004, ApJ, 607, L87
De Lucia G., Blaizot J., 2007, MNRAS, 375, 2 (DLB07)
De Lucia G., Kauffmann G., White S. D. M., 2004, MNRAS, 349, 1101
de Vaucouleurs G., de Vaucouleurs A., Corwin H. G., Jr, Buta R. J., Paturel G., Fouque P., 1991, Third Reference Catalogue of Bright Galaxies, Vol. 1–3, XII. Springer-Verlag, Berlin, p. 2069
Desert F.-X., Boulanger F., Puget J. L., 1990, A&A, 237, 215
Devriendt J. E. G., Guiderdoni B., 2000, A&A, 363, 851
Devriendt J. E. G., Guiderdoni B., Sadat R., 1999, A&A, 350, 381
Dole H. et al., 2001, A&A, 372, 364
Dorschner J., Henning T., 1995, A&AR, 6, 271
Draine B. T., 2003, ApJ, 598, 1017
Draine B. T., Anderson N., 1985, ApJ, 292, 494
Driver S. P., Popescu C. C., Tuffs R. J., Liske J., Graham A. W., Allen P. D., de Propris R., 2007, MNRAS, 379, 1022
Dwek E. et al., 1997, ApJ, 475, 565
Efstathiou A., Rowan-Robinson M., 1995, MNRAS, 273, 649
Elbaz D. et al., 1999, A&A, 351, L37
Elbaz D., Cesarsky C. J., Chanial P., Aussel H., Franceschini A., Fadda D., Chary R. R., 2002, A&A, 384, 848
Ferrara A., Bianchi S., Cimatti A., Giovanardi C., 1999, ApJS, 123, 437
Fioc M., Rocca-Volmerange B., 1997, A&A, 326, 950
Fontana A. et al., 2006, A&A, 459, 745
Fontanot F., Monaco P., Cristiani S., Tozzi P., 2006, MNRAS, 373, 1173
Fontanot F., Monaco P., Silva L., Grazian A., 2007, MNRAS, 382, 903
Fitzpatrick E., 1989, in Allamandola L. J., Tielens A. G. G. M., eds, Proc. IAU Symp. 135, Interstellar Dust. Kluwer, Dordrecht, p. 37
Fitzpatrick E. L., 1999, PASP, 111, 63
Fitzpatrick E. L., Massa D., 2007, ApJ, 663, 320
Giovanelli R., Haynes M. P., Salzer J. J., Wegner G., da Costa L. N., Freudling W., 1995, AJ, 110, 1059
Gordon K. D., Calzetti D., Witt A. N., 1997, ApJ, 487
Graham A. W., 2001, MNRAS, 326, 543
Granato G., Lacey C. G., Silva L., Bressan A., Baugh C. M., Cole S., Frenk C. S., 2000, ApJ, 542, 710
Granato G. L., De Zotti G., Silva L., Bressan A., Danese L., 2004, ApJ, 600, 580
Gruppioni C., Lari C., Pozzi F., Zamorani G., Franceschini A., Oliver S., Rowan-Robinson M., Serjeant S., 2002, MNRAS, 335, 831
Guiderdoni B., Rocca-Volmerange B., 1987, A&A, 186, 1 (GRV87)
Guiderdoni B., Hivon E., Bouchet F. R., Maffei B., 1998, MNRAS, 295, 877
Hatton S., Devriendt J. E. G., Ninin S., Bouchet F. R., Guiderdoni B., Vibert D., 2003, MNRAS, 343, 75
Hauser M. G. et al., 1998, ApJ, 508, 25
Hauser M. G., Dwek E., 2001, ARA&A, 39, 249
Hughes D. H. et al., 1998, Nat, 394, 241
Inoue A. K., 2005, MNRAS, 359, 171
Inoue A. K., Buat V., Burgarella D., Panuzzo P., Takeuchi T. T., Iglesias-Paramo J. I., 2006, MNRAS, 370, 380
Jonsson P., 2006, MNRAS, 372, 2
Jonsson P., Cox T. J., Primack J. R., Somerville R. S., 2006, ApJ, 637, 255
Kang X., Jing Y. P., Mo H. J., Börner G., 2005, ApJ, 631, 21
Kauffmann G., Colberg J. M., Diaferio A., White S. D. M., 1999, MNRAS, 303, 188
Kaviani A., Haehnelt M. G., Kauffmann G., 2003, MNRAS, 340, 739
Kitzbichler M. G., White S. D. M., 2007, MNRAS, 376, 2
Kong X., Charlot S., Brinchmann J., Fall S. M., 2004, 349, 769
Kuchinski L. E., Terndrup D. M., Gordon K. D., Witt A. N., 1998, AJ, 115, 1438
Kylafis N. D., Bahcall J. N., 1987, ApJ, 317, 637
Lacey C., Guiderdoni B., Rocca-Volmerange B., Silk J., 1993, ApJ, 402, 15
Lacey C. G., Baugh C. M., Frenk C. S., Silva L., Granato G. L., Bressan A., 2008, MNRAS, 385, 1155
Le Floc'h E. et al., 2005, ApJ, 632, 169
Leitherer C. et al., 1999, ApJS, 123, 3
Lucy L. B., Danziger I. J., Gouiffes C., Bouchet P., 1991, in Woosley S.E., ed., Supernovae. Springer-Verlag, New York, p. 82
Li A., Draine B. T., 2001, ApJ, 554, 778
Madgwick D. S., Somerville R., Lahav O., Ellis R., 2003, MNRAS, 343, 871
Maiolino R., Schneider R., Oliva E., Bianchi S., Ferrara A., Mannucci F., Pedani M., Roca Sogorb M., 2004, Nat, 431, 533
Masters K. L., Giovanelli R., Haynes M. P., 2003, AJ, 126, 158
Mathis J. S., 1990, ARA&A, 28, 37
Mathis J. S., Mezger P. G., Panagia N., 1983, A&A, 128, 212
Mathis H., Lemson G., Springel V., Kauffmann G., White S. D. M., Eldar A., Dekel A., 2002, MNRAS, 333, 739
Mo H. J., Mao S., White S. D. M., 1998, MNRAS, 295, 319
Möllenhoff C., Popescu C. C., Tuffs R. J., 2006, A&A, 456, 941
Monaco P., 2004, MNRAS, 352, 181
Monaco P., Fontanot F., 2005, MNRAS, 359, 283
Monaco P., Murante G., Borgani S., Fontanot F., 2006, ApJ, 652, L89
Monaco P., Fontanot F., Taffoni G., 2007, MNRAS, 375, 1189
Moriondo G., Giovanelli R., Haynes M. P., 1998, A&A, 338, 795
Nagashima M., Totani T., Gouda N., Yoshii Y., 2001, ApJ, 557, 505
Natta A., Panagia N., 1984, ApJ, 287, 228
Osterbrock D. E., 1989, Astrophysics of Gaseous Nebulae and Active Galactic Nuclei. Univ. Science Books, Mill Valley, CA
Panuzzo P., Bressan A., Granato G. L., Silva L., Danese L., 2003, A&A, 409, 99
Panuzzo P., Granato G. L., Buat V., Inoue A. K., Silva L., Iglesias-Paramo J., Bressan A., 2007, MNRAS, 375, 640
Pierini D., Gordon K. D., Witt A. N., Madsen G. J., 2004, ApJ, 617, 1022
Popescu C. C., Tuffs R. J., 2002, MNRAS, 335, L41
Popescu C. C., Misiriotis A., Kylafis N. D., Tuffs R. J., Fischera J., 2000, A&A, 362, 138
Popescu C. C. et al., 2005, ApJ, 619, L75
Puget J.-L., Abergel A., Bernard J.-P., Boulanger F., Burton W. B., Desert F.-X., Hartmann D., 1996, A&A, 308, L5
Rocha M., Jonsson P., Primack J. R., Cox T. J., 2008, MNRAS, 383, 1281
Rowan-Robinson M., 1986, MNRAS, 219, 737
Salpeter E. E., 1955, ApJ, 121, 61
Sanders D. B., Mirabel I. F., 1996, ARA&A, 34, 749
Silva L., 1999, PhD thesis, SISSA, Trieste
Silva L., Granato G. L., Bressan A., Danese L., 1998, ApJ, 509, 103
Silva L., De Zotti G., Granato G. L., Maiolino R., Danese L., 2005, MNRAS, 357, 1295
Smail I., Ivison R., Blain A., 1997, ApJ, 490, L5
Smail I., Ivison R., Blain A., Kneib J.-P., 2002, MNRAS, 331, 495
Soifer B. T., Neugebauer G., 1991, AJ, 101, 354
Somerville R. S., Primack J. R., 1999, MNRAS, 310, 1087
Tuffs R. J., Popescu C. C., Völk H. J., Kylafis N. D., Dopita M. A., 2004, A&A, 419, 821
Tully R. B., Pierce M. J., Huang J.-S., Saunders W., Verheijen M. A. W., Witchalls P. L., 1998, AJ, 115, 2264
Városi F., Dwek E., 1999, ApJ, 523, 265
Vega O., Silva L., Panuzzo P., Bressan A., Granato G. L., Chavez M., 2005, MNRAS, 364, 1286
Viola M., Monaco P., Borgani S., Murante G., Tornatore L., 2008, MNRAS, 383, 777
Wang B., Heckman T. M., 1996, ApJ, 457, 645
White S. D. M., Frenk C. S., 1991, ApJ, 379, 52
Witt A. N., Thronson H. A. Jr, Capuano J. M. Jr, 1992, ApJ, 393, 611
Xilouris E. M., Byun Y. I., Kylafis N. D., Paleologou E. V., Papamastorakis J., 1999, A&A, 344, 868
Zubko V., Dwek E., Arendt R. G., 2004, ApJS, 152, 211

This paper has been typeset from a TEX/LATEX file prepared by the author.